LA-UR-15-27789 (Accepted Manuscript)

Source and seed populations for relativistic electrons: Their roles in radiation belt changes

Jaynes, A.; Baker, D.; Singer, H.; Rodriguez, J.; Loto'aniu, T.; Ali, A.; Elkington, S.; Li, X.; Kenekal, S.; Fennell, J.; Li, W.; Thorne, R.; Kletzing, C.; Spence, S.; Reeves, Geoffrey D.

To be published in: JOURNAL OF GEOPHYSICAL RESEARCH-SPACE PHYSICS, Vol.120, iss.9, p.7240-7254, SEP 2015.

DOI to publisher's version: 10.1002/2015JA021234

Permalink to record: http://permalink.lanl.gov/object/view?what=info:lanl-repo/lareport/LA-UR-15-27789

Source and Seed Populations for Relativistic Electrons: Their Roles in Radiation Belt Changes

A.N. Jaynes[1], D.N. Baker[1], H.J. Singer[2], J.V. Rodriguez[3,4], T.M. Loto'aniu[3,4], A. F. Ali[1], S.R. Elkington[1], X. Li[1], S.G. Kanekal[5], J.F. Fennell[6], W. Li[7], R.M. Thorne[7], C.A. Kletzing[8], H.E. Spence[9], and G.D. Reeves[10]

[1]Laboratory for Atmospheric and Space Physics, University of Colorado, Boulder, CO 80303

[2] NOAA Space Weather Prediction Center, Boulder, CO 80305.

[3] Cooperative Institute for Research in Environmental Sciences, University of Colorado, Boulder, CO 80309.

[4] NOAA National Centers for Environmental Information, Boulder, CO 80305.

[5] NASA/Goddard Space Flight Center, Greenbelt, MD 20771.

[6] Space Sciences Department, The Aerospace Corporation, Los Angeles, CA 90009.

[7] Dept. of Atmospheric and Oceanic Sciences, University of California, Los Angeles, CA 90095.

[8] Department of Physics and Astronomy, University of Iowa, Iowa City, IA 52242.

[9] Institute for Study of Earth, Oceans, and Space, University of New Hampshire, Durham, NH 03824.

[10] Space Science and Applications Group, Los Alamos National Laboratory, Los Alamos, NM 87545.

Corresponding Author: A. N. Jaynes, LASP, University of Colorado Boulder, Boulder, CO 80455, USA (Allison.Jaynes@lasp.colorado.edu)

Key Points

- Source/seed energy electrons required to produce MeV radiation belt energization
- Substorm injections lead to VLF wave growth, producing MeV acceleration
- ULF waves may enhance loss/accel. due to increased outward/inward diffusion

Index Terms 2774, 2788, 2730, 2720, 2772

Keywords radiation belts, Van Allen Probes, relativistic electrons, VLF waves, ULF waves, substorms

Abstract Strong enhancements of outer Van Allen belt electrons have been shown to have a clear dependence on solar wind speed and on the duration of southward interplanetary magnetic field. However, individual case study analyses also have demonstrated that many geomagnetic storms produce little in the way of outer belt enhancements and, in fact, may produce substantial losses of relativistic electrons. In this study, focused upon a key period in August-September 2014, we use GOES geostationary orbit electron flux data and Van Allen Probes particle and fields data to study the process of radiation belt electron acceleration. One particular interval, 13-22 September, initiated by a short-lived geomagnetic storm and characterized by a long period of primarily northward IMF, showed strong depletion of relativistic electrons (including an unprecedented observation of long-lasting depletion at geostationary orbit) while an immediately preceding, and another immediately subsequent, storm showed strong radiation belt enhancement. We demonstrate with these data that two distinct electron populations resulting from magnetospheric substorm activity are crucial elements in the ultimate acceleration of highly relativistic electrons in the outer belt: the source population (tens of keV) that give rise to VLF wave growth; and the seed population (hundreds of keV) that are, in turn, accelerated through

VLF wave interactions to much higher energies. ULF waves may also play a role by either inhibiting or enhancing this process through radial diffusion effects. If any components of the inner magnetospheric accelerator happen to be absent, the relativistic radiation belt enhancement fails to materialize.

1. Introduction

Early studies of high-energy electrons at geostationary orbit (L~6.6) showed a clear relationship between episodes of high-speed solar wind and subsequent relativistic electron enhancements [*Paulikas and Blake*, 1979; *Baker et al.*, 1979]. This led to the view that magnetospheric substorm activity driven by high solar wind speed played a key role in providing "seed" electrons of energy up to a few hundred keV in kinetic energy [*Baker et al.*, 1986]. Studies based upon data from the SAMPEX (Solar, Anomalous, and Magnetospheric Particle Explorer) and POLAR missions also showed that high-speed solar wind streams were effective at producing outer radiation belt electron flux enhancements [*Baker et al.*, 1997a; *Kanekal et al.*, 1999]. Using data from the Highly Elliptical Orbit (HEO) spacecraft, it was also shown that for strong relativistic electron acceleration to occur throughout the entire outer zone, the solar wind was required to have southward interplanetary magnetic field (IMF) directionality [*Blake et al.*, 1997].

Studies related to this early work demonstrated on a statistical basis that many geomagnetic storms produced relativistic electron flux enhancements at GEO (geostationary orbit), but many other storms did not [*Summers et al.*, 2004; *Hudson et al.*, 2008]. *Reeves et al.* [2003a], specifically, showed that ~50% of storms over a several year period exhibited a high-energy electron flux increase while ~25% showed an actual flux decrease during strong storm activity.

69 The remaining 25% of cases showed essentially no flux change between the pre-storm levels and
70 the post-storm levels. Studies of the "total radiation belt content" [*Baker et al.,* 2004] and a more
71 extended study of GEO flux relations to solar wind drivers [*Reeves et al.,* 2011] found that the
72 relativistic electron-solar wind speed relationship is not a simple linear one. For example, *Reeves*
73 *et al.* [2011] found that a scatter plot of electron flux and solar wind speed formed a "triangle"
74 with a speed-dependent lower limit to fluxes but a speed-independent upper limit. Further
75 analysis of the same data set [*Li et al.*, 2011] compared 15 years of solar wind data to GEO
76 observations of MeV electron flux and found that high solar wind speeds are not necessary for
77 MeV enhancements; instead, southward IMF is the essential condition to cause acceleration of
78 MeV electrons in the outer radiation belt.

79 The Van Allen Probes pair of NASA spacecraft were launched on 30 August 2012. These
80 spacecraft have ideal instruments to measure the relativistic electron component throughout the
81 Van Allen zones. The Relativistic Electron-Proton Telescope (REPT) investigation [*Baker et al.*,
82 2012] measures ~1 to 20 MeV electrons. The Van Allen Probes also have the Magnetic Electron-
83 Ion Spectrometer (MagEIS) investigation [*Blake et al.*, 2013] to measure low- and medium-
84 energy (~30 keV - ~1MeV) electrons and complete wave data from the Electric and Magnetic
85 Field Instrument Suite and Integrated Science (EMFISIS) experiment [*Kletzing et al.*, 2013].
86 Together the overall Van Allen Probes payload has given an unprecedented view of the
87 acceleration, transport, and loss of radiation belt particles.

88 Early results from the Van Allen Probes mission revealed unexpected morphological features
89 of the Van Allen belts such as a transient third belt or "storage ring" feature [*Baker et al.*, 2013].
90 This previously unreported aspect of the outer trapping region has been studied in detail
91 theoretically [*Thorne et al.*, 2013a], and had been previously observed only in proton data

92 [*Hudson et al.*, 1997], not electron populations. Another surprising structural feature of the ultra
93 relativistic electron distribution is the extremely sharp inner edge of the outer zone at L=2.8
94 [*Baker et al.*, 2014a]. This work has clearly shown that very strong spatial gradients can persist
95 for long periods in high-energy electron radiation belt distributions. Consequently, the inner zone
96 is shielded from inward radial diffusion and is largely devoid of electrons at energies E≳1 MeV
97 [*Baker et al.*, 2014a; *Li et al.*, 2015; *Fennell et al.*, 2015].

98 Detailed studies of specific events using the dual Van Allen Probes have shown the way in
99 which strong geomagnetic storms can accelerate electrons to relativistic energies. *Reeves et al.*
100 [2013] studied a powerful storm in October 2012 that exhibited "local" acceleration due to
101 chorus-wave interactions with seed electrons at L~4.2. This was modeled by *Thorne et al.*
102 [2013b] to show very good quantitative understanding of the wave-particle acceleration
103 mechanism. *Baker et al.* [2014b] studied a period in March 2013 that exhibited both a relatively
104 gradual acceleration event due to a high-speed solar wind stream as well as a separate, very
105 abrupt local acceleration event driven by impact of a strong solar coronal mass ejection (CME).
106 *Foster et al.* [2014] in a companion paper to the *Baker et al.* [2014b] study showed that an
107 intense magnetospheric substorm event played a key and central role in the abrupt relativistic
108 electron acceleration event in March 2013. Again, this particular event occurred deep within the
109 outer radiation belt associated with chorus wave interactions as in the *Reeves et al.* [2013] event.

110 Based on the already extensive studies of outer zone electron acceleration from the Van
111 Allen Probes mission, we have been curious to examine cases where elements of the overall
112 acceleration scenario were missing. An ideal situation presented itself when observations from
113 the Geostationary Operational Environmental Satellite (GOES) spacecraft [*Onsager et al.*, 1996;
114 *Singer et al.*, 1996] showed an extended, and rather unexpected, anti-correlation of solar wind

speed with GEO relativistic electron fluxes. This period in September 2014 is the focus of our detailed, multi-satellite study reported here.

2. Electron Local "Heating" Acceleration Mechanism

While earlier studies have previously implied this mechanism [e.g. *Green and Kivelson,* 2004b; *Chen et al.,* 2006], several recent studies have documented the indisputable occurrence of localized acceleration of energetic electrons to multi-MeV energies deep within the outer radiation belt ($3.5 \lesssim L \lesssim 5.0$). These studies [*Reeves et al.*, 2013; *Baker et al.*, 2014b; *Foster et al.*, 2014] have been bolstered by theoretical modeling [e.g., *Thorne et al.,* 2013b; *Li et al.,* 2014; *Tu et al.*, 2014] to show that low-energy (few to tens of keV) electrons can fuel the growth of chorus waves that, in turn, can act on even more energetic (tens to hundreds of keV) substorm-injected electrons to produce relativistic electrons in the outer zone. This mechanism can operate on quite short time scales.

Figure 1 shows a schematic diagram of the key ingredients of the local acceleration mechanism. An isolated event exhibiting this local heating process normally begins with a strong solar wind forcing event: This typically would be a strong southward turning of the IMF which then loads substantial energy into the Earth's magnetotail. This in turn leads to a strong magnetospheric substorm onset after about a one-hour long growth phase [*McPherron et al.*, 1973]. The substorm onset almost invariably is accompanied by an injection of low- to medium-energy electrons into the Earth's inner magnetosphere [e.g., *Baker et al.*, 1996 and references therein]. We generally describe the hot plasma (~1 keV) and lower-energy energetic electrons (tens of keV) in substorm events as the "source" population of particles. As discussed by *Thorne et al.* [2013b and references therein], this source population of electrons has anisotropic angular

distributions that feed free energy into electromagnetic waves in the lower chorus band. Such chorus waves can, in turn, interact resonantly with higher energy (30~300 keV) electrons also injected by substorms. We call these medium-energy electrons the "seed" population of particles. Chorus waves Doppler-shifted to the cyclotron frequency of the seed population electrons can very efficiently heat (and accelerate) such electrons to multi-MeV energies through resonant interactions [e.g., *Boyd et al.*, 2014]. As shown in Figure 1, substorms are necessary to produce the initial energetic electron population. Thereafter amplified chorus waves transfer energy from the source electrons to a portion of the seed electrons. These seed electrons can be pumped up in energy by large factors on characteristic time scales of minutes to hours [*Summers et al.*, 2002; *Horne et al.*, 2005; *Thorne et al.*, 2013b; *Summers et al.*, 2012].

A question we wish to address in the present paper is: what happens if key elements of the acceleration mechanism portrayed in Figure 1 are absent altogether or are taken away at some point in an acceleration sequence? Can we use geostationary orbit, Van Allen Probes, and other data to look at weak or interrupted acceleration events when key steps in the progression do not materialize? Examining such alternative scenarios helps us gain a deeper understanding of how the "normal" acceleration events really work.

3. August-September 2014 Event Overview

Our first recognition of an unusual and quite long-lasting depletion of relativistic electrons in the outer radiation belt came from the real-time operational GOES data at geostationary orbit. Figure 2 provides in the upper panels a long run of GOES-13 Magnetospheric Electron Detector (MAGED) data [*Hanser*, 2011] for the period 1 August 2014 to 15 October 2014 from Telescope 5 whose center pitch angle is close to 90 degrees during most of the period. The lowest energy

channel (plotted as the black trace in Figure 2) is for 30 to 50 keV electrons. The GOES-13 E>2.0 MeV electron fluxes, used by the NOAA Space Weather Prediction Center for its real-time alerts when the flux exceeds 1000 cm^{-2} $s^{-1}sr^{-1}$, are shown by the purple colored trace in Figure 2. The light brown coloration associated with the E>2.0 MeV measurements in the figure is for times when the background rate in that channel was greater than 30% of the observed total count rate. The background level in the E>2.0 MeV electron channel is estimated using the empirical expression used by SWPC (Space Weather Prediction Center) in its real time processing of this channel, which consists of a linear combination of the fluxes from four GOES solar proton channels between 8.7 and 200 MeV. For details please refer to Rodriguez [2014]. During most of the period shown in Figure 2., the backgrounds were due to the slowly-varying galactic cosmic ray flux, the exception being 11-13 September, when a weak solar energetic particle (SEP) event occurred. During this period, GOES-13 is at local midnight at approximately 05 UT.

A striking diminution of E>2.0 MeV electrons below the background level was observed during the period 13 September to 22 September 2014. Such reductions at geostationary orbit, usually of shorter duration than this case, have been reported previously and have been studied extensively [*Onsager et al.*, 2002, 2007; *Green et al.*, 2004]. However, to our knowledge such a deep and long-lasting decrease of relativistic electrons at GEO as this one has not been reported previously. During the entire period shown in Figure 2, the north-south component of the GOES-13 magnetic field (not shown) was positive, indicating that the GOES-13 spacecraft was located inside the magnetopause [*Rufenach et al.*, 1989], while the E>2 MeV electron fluxes were below background levels during 13-22 September. Therefore, the observations show that the trapped

E>2 MeV electron population in the magnetosphere—at least near GEO—was greatly depleted and was below GOES instrument background levels for nearly 10 days.

In the lower portion of Figure 2 we show an expanded view of the GOES-13 data for the period 8 September through 25 September 2014. These data demonstrate that electrons in the lower energy ranges (30-200 keV) also were quite reduced in flux levels beginning on 13 September and extending to 16 September. Not until the middle of 16 September did one see a return to the pattern of spikey bursts of these medium-energy electrons. Such bursts are closely associated with substorm injection events [*Baker et al.*, 1996; *Sergeev et al.*, 2015]. From the long run of data shown in Figure 2, we would conclude that the period from 13 to 22 September was remarkably devoid of E>2 MeV electrons and was also quite reduced in the flux and occurrence frequency of substorm-injected medium-energy seed electrons.

The solar wind, IMF, and geomagnetic conditions as they relate to the geostationary orbit electron flux data just described are shown in Figure 3. The upper panel presents the auroral electrojet (AE) index, the geomagnetic storm (Dst) index, the solar wind dynamic pressure (P), the IMF north-south (B_z) component, and the solar wind speed (V) for the period 25 August through 4 October 2014. The lower portion of Figure 3 shows these same quantities on an expanded time scale for 8-26 September.

A dominant feature of the data portrayed in Figure 3 is the high-speed solar wind stream that was observed beginning on 12 September and lasting until ~16 September. The peak solar wind speed was >700 km/sec and the speed remained relatively high (≳500 km/sec) for several days. Based on research cited previously [e.g., *Baker et al.*, 1986, 1997a] we would have expected this stream to produce a large, long-lasting enhancement of relativistic electrons at GEO; instead (as shown in Figure 2) the E>2 MeV fluxes were quite depleted.

Other features of the solar wind and geomagnetic drivers for this period are interesting as well. Note in Figure 3 that the leading edge of the high-speed solar wind stream was accompanied by high dynamic solar wind pressure (reaching nearly 20 nPa late on 12 September), potentially indicating a CME (coronal mass ejection) embedded within the HSS. The north-south component of the GOES-15 magnetic field (not shown) went strongly negative between 2218 and 2223 UT on 12 September when the satellite was ~1.5 hrs past local noon, indicating that the magnetopause was briefly pushed inward of geostationary orbit [*Rufenach et al.*, 1989]. The increased solar wind speed and dynamic pressure drove strong geomagnetic activity (AE ~1000 nT and Dst ~-90 nT) at that same time. However, abruptly after this peak of geomagnetic activity, the IMF turned strongly northward and it remained so for over a day. In fact, the IMF remained at least weakly northward for most of the period 13-21 September. This prolonged northward IMF—especially on 13-15 September—reduced the AE level to virtually zero. This absence of substorm activity explains the absence of seed population injections witnessed in the GOES-13 data (Figure 2) as discussed above and, most likely, the absence of "source" population electrons as well.

The period 13 September to roughly 20 September contrasts strikingly with periods preceding (27 August – 7 September) and succeeding (22 September – 2 October) the interval of our central attention. Both of these other "bracketing" time intervals had high, almost continuously fluctuating levels of geomagnetic activity (as measured by the AE index). In fact, both of these adjacent periods are quite similar to the pattern termed "high-intensity, long-duration, continuous AE activity" (HILDCAA) intervals [*Tsurutani et al.*, 1995]. As noted in recent studies [*Miyoshi et al.*, 2008; *Hajra et al.*, 2015], HILDCAA events can often be quite effective at producing high-energy electrons at geostationary orbit. This is well borne out by

examination of the GOES-13 data in Figure 2 and by comparing those data with the AE and IMF records in Figure 3. Additionally, in Figure 4, the 27 August event appears to be a particularly well-behaved acceleration event, with source energy electrons appearing prior to seed and MeV populations, and sustaining high fluxes well into the build-up of the MeV belt.

A broader view of energetic electron properties throughout the outer radiation belt is shown in Figure 4 based on Van Allen Probes measurements. This multi-panel plot shows color-coded intensities of electrons in various selected energy ranges from ~5 keV (top panel) to 5.6 MeV (lower panel) for the period 25 August through 4 October 2014, from the Van Allen Probes RBSP-ECT instrument suite [*Spence et al.*, 2013]. The top panel is from the HOPE experiment [*Funsten et al., 2013]*, the next three panels are from the MagEIS experiment [*Blake et al.*, 2013], and the lower three panels are from the REPT experiment [*Baker et al.*, 2013]. The data are portrayed as a function of [*McIlwain*, 1996] L-parameter (vertical axis) and time (horizontal axis) for each energy range. During this period, the apogee of the Van Allen Probes was located near 5.5 MLT, and the local time coverage above L=4.0 encompassed the dawn sector covering ~1.5-8.5 MLT.

As is evident from Figure 4, electrons from a few keV to several MeV were all concurrently depleted early on 27 August at the beginning of the Dst and AE enhancement on that date (see Figure 3). Thereafter, progressively higher and higher energy particles built up in flux throughout the days of 27 August and 28 August. This enhancement of electron intensity occurred from L~3.5 out to the edge of the radiation belt sampled by Van Allen Probes ($L \gtrsim 6.5$). High-energy electron flux enhancement persisted until 13 September. As was noted above, the electron enhancement seen throughout most of the outer zone from 27 August to ~7 September

was closely associated with the HILDCAA-like period identified in the simultaneous AE and IMF data (Figure 3).

Given the strong solar wind speed increase on 12 September, we would have expected a large further relativistic electron flux increase on 13 September and the days following. Instead, the fluxes measured by the Van Allen Probes at energies from ~1 MeV to at least 7 MeV were seen to have been strongly depleted. This depletion lasted from the beginning of 13 September to 22-24 September (depending on particle energy). The flux reduction seen by the Van Allen Probes sensors comports very well with the flux reduction interval also seen by GOES-13 (see Figure 2) as described previously.

From Figure 4 it is seen that the ~5 keV and ~30 keV electrons were diminished over essentially all L-shells (panel 4a) on 13 September and largely remained so until ~19 September. This is indicative of the source electron population being substantially reduced in association with the dropout of relativistic electrons. On the other hand – and somewhat curiously – the ~350 keV electrons (panel 4b) appears to be rapidly transported deeper into the outer zone over the period 12 September into 13 September, meaning that the seed population was actually enhanced during the period 13-16 September (at least for $3.0 \leq L \leq 4.5$). Short-lived depletions for ~350 keV at 90° pitch angles are evident just after the storm main phase (Figure 5), though they are quickly built up to pre-storm levels within hours. Thus, it can be the case that source electrons and relativistic electrons can be depleted in the long-term even while seed electrons get (at least locally) enhanced. The distinctly different behavior between the 350 keV (seed) electrons and those at higher (>MeV) energy is probably related to the prevailing radial phase space density (PSD) gradient. Electrons with magnetic moment below a few hundred MeV/G have a positive radial gradient, while those with higher magnetic moment develop peaks near L ~ 4-4.5

associated with local acceleration during the previous magnetic storm. As demonstrated later in Section 5, during the period around September 13 there was a considerable increase in ULF wave activity, which would rapidly drive lower energy electrons inward and lead to enhanced flux at lower L as observed. The increase in radial diffusion would also drive relativistic electrons outside the PSD peak towards the magnetopause boundary where they would be lost by magnetopause shadowing. Removal of the relativistic population inside the PSD peak may require another mechanism such as loss to the atmosphere by EMIC scattering, but confirmation of this will require detailed quantitative modeling.

Note in Figure 4 that on 22 September to late 24 September (depending on electron energy), the relativistic electron populations were substantially restored to high intensity levels. This restoration corresponded to a clear period of strong AE activity and, hence, to further HILDCAA-like behavior. High electron fluxes continued to be seen until ~4 October in association with the elevated AE and solar wind activity. Comparing Figure 2 with Figure 4, we again note that the electron behavior for the broad range of L-values sampled by the Van Allen Probes instruments comports well with the electron fluxes measured at the more limited L-range sampled by GOES-13.

4. Detailed Examination of the 12-24 September Depletion Event

The rapid decrease of radiation belt electrons late on 12 September shown in Figure 4 is quite distinctive. The decrease was observed at energies of a few keV as well as from ~1 MeV up to the multi-MeV range. In Figure 5 we show pitch angle versus time plots, color-coded by flux intensity, for several selected Van Allen Probes energy channels. We see that beginning at ~1950 UT on 12 September and for the next several hours, the electrons measured by sensors on the

297 RBSP-A spacecraft showed strong minima at 90° pitch angles at L>6. This is consistent with the
298 magnetopause "shadowing" mechanism [e.g. *Wilken et al.*, 1982; *Turner et al.*, 2012; *Hietala et*
299 *al.*, 2014] and suggests that the radiation belt depletion was caused by particles being lost
300 through the dayside magnetospheric boundary. This picture is supported by two pieces of
301 evidence: (1) the *Shue et al.* [1998] model gives a magnetopause stand-off distance close to
302 GEO for several hours during the depletion event, and (2) the enhancement in ULF wave power
303 during this time is sufficient to drive this process (discussed further in the next section). As
304 expected, similar pitch angle distributions for GOES-13 [*Hartley et al.*, 2013] in the 30-200 keV
305 electron energy range (Figure 6) also show such depletions in the 90° pitch angle range. Notably,
306 this figure demonstrates that overall electron intensities at GEO in this energy range were much
307 reduced from 13 September onward.
308
309 **5. Observed Wave Activity**
310 From the scenario portrayed in Figure 1, we would expect that an absence of substorm
311 activity on 13 September and on subsequent days would mean that the source populations of
312 electrons would be quite reduced. Without ample source electrons to supply free energy, the
313 chorus wave activity should diminish greatly as well. Figure 7 shows EMFISIS wave data for 12-
314 14 September and for 21-23 September. The upper panels for the time of radiation belt depletion
315 (late on 12 September into 13 September) show that lower band chorus went away almost
316 completely on 13 and 14 September in the vicinity of the Van Allen Probes. This remained
317 largely the case (data not shown here) until 22 September when the lower band chorus re-
318 emerged (see lower panels in Figure 7).

A more global indicator of chorus wave activity comes from Polar Orbiting Environmental Satellite (POES) data. This recently developed technique [*Li et al.*, 2013] uses POES electron precipitation data over 30-100 keV to infer chorus wave intensity. Figure 8 shows that, indeed, chorus wave activity was strong until late on 12 September and early on 13 September. Wave activity then was minimal at all MLT sectors from later on 13 September through 18 September. A brief episode of chorus enhancement occurred on 19-21 September, but strong chorus resurgence did not occur until 22 September. This is when GOES saw a return of substorm electron injections (Figure 2) and when the AE index again became enhanced (see Figure 3). These injections and enhanced AE activity occurred after the fluctuating Bz component of the IMF turned weakly southward at approximately 02 UT on 22 September, never decreasing below -5 nT for the rest of the day.

The contribution to this process as a whole by ultra-low frequency (ULF) waves is likely an enhancement or suppression of individual episodes in the normal sequence depending on the phase space density gradient and the magnetopause location. Figure 9 shows an overview of the Pc5 ULF power in the compressional component as observed in-situ by the Van Allen Probes' EMFISIS fluxgate magnetometers. The figure indicates that both spacecraft saw almost identical ULF wave activity that can be summarized as follows. The Pc5 power was enhanced during the main phase of the 12 September storm, and lasted through 13 September before settling at pre-storm levels. The power spectral density peak occurs at approximately 5-6 mHz over the orbit of enhanced power from 12-13 September. At this frequency, for a drift resonance condition given as: $\omega_{wave} = m_{wave}\omega_{drift}$, and assuming m=1, we expect resonance for electrons with energies of 5 MeV to >8 MeV. However, with higher mode numbers, the resonant energy can decrease to as low as 100's of keV. Indeed, a distribution of mode numbers is possible up to m>15, particularly

342 during times of high speed solar wind [*Elkington et al.*, 2012; *Claudepierre et al.*, 2008]. Thus,
343 ULF waves may have played a direct role in the disappearance of the outer belt on 13 September
344 by driving outward radial diffusion from multi-MeV energies down to seed population energies.
345 ULF power is again enhanced following 24 September, during the reappearance of the MeV
346 outer belt. Similarly to the previous episode, the observed ULF peak frequencies would most
347 readily resonate with multi-MeV to 100's of keV electrons. ULF waves may be partly
348 responsible for the rebuilding of the outer belt after 24 September. However, the chorus waves
349 reappear at an earlier time, on 22 September, as the Van Allen Probes start to observe
350 acceleration occurring over a wide energy range. Until a deeper analysis is performed, the effect
351 of the enhanced ULF wave power on the particle energization or inward diffusion is not
352 immediately straightforward.
353
354 **6. Spectral Changes During Storm Times**
355 Early work at GEO [e.g., *Baker et al.*, 1986] suggested that energetic electron spectra could
356 be adequately approximated as simple power law distributions. During the period of high solar
357 wind speed and strong substorm activity, it was inferred that a steep power law was appropriate.
358 This meant there were copious quantities of lower energy (source and seed) electrons, while on
359 the trailing edge of high-speed streams the spectrum was much harder with large relative
360 enhancement of electrons in the MeV and multi-MeV range. The comprehensive measurements
361 from the Van Allen Probes sensors (MagEIS and REPT) allow us to examine more thoroughly
362 such spectral properties throughout the course of both enhancement and depletion events.
363 Figure 10 shows composite energy spectra at L=4.5 beginning on 9 September before the
364 outer belt depletion all the way through to after the restoration of the relativistic population on 27

September. We see from the high-resolution spectral data that the energy distributions cannot typically be described as simple power laws. Instead, during times of active solar wind forcing (12-14 September and 19-21 September) the spectrum is better described as an exponential ($j = j_0 e^{-E/E_0}$) spectrum. During the times of relativistic electron enhancement (9-10 September and 21-23 September) the spectrum is quite remarkable with a broad, almost flat characteristic from below E~100 keV all the way to E~1.0 MeV. Only above E=1 MeV are the electron fluxes elevated.

After the relativistic electron dropout during the 12 September storm, the 10's of keV source population continues to decline, yet the 100's of keV seed population remains elevated until a dramatic drop on 17 September, as was noted earlier. From 19 September onward, when the high-speed stream reaches the magnetosphere, the seed population remains high, then drops, then regains higher flux levels after 25 September. In this way, the behavior of the seed energies is very similar between the 12 September and the 19 September storms. However, the behavior of the source population at the lowest energy range is very different over the two events. The 10's of keV source energy electrons show essentially no change from 19 September through 27 September. With the source population level remaining high, the chorus waves are able to grow and, over time, accelerate the seed population to the MeV energies that are seen returning after 22 September. This novel look at the high-resolution energy spectrum in the outer radiation belt presents the picture of three distinct electron populations; a departure from the previous portrayal of two power law spectra that join in the 100's of keV region. Careful observation reveals a full radiation belt electron spectrum that often shows a plateau in the middle energy regime and revolves or rocks around 600-700 keV throughout varying solar wind and geomagnetic activity.

7. Discussion and Conclusions

388 Early research discussed previously in this paper established that a prevalent pattern of solar
389 wind-magnetosphere coupling occurs during strong solar wind forcing events. In this pattern,
390 high solar wind speed leads to strong substorm activity and from this there emerges a
391 source/seed population of electrons that ordinarily is further processed within the magnetosphere
392 to produce a relativistic electron population throughout much of the outer radiation zone. This
393 sequence occurs commonly enough that linear prediction filter analysis has revealed the "transfer
394 function" between solar wind drivers and radiation belt responses [*Baker et al.*, 1990]. By
395 convolving the prediction filter response function with the measured upstream solar wind speed,
396 for example, the linear prediction filter can provide a several day forecast of expected relativistic
397 electron fluxes at GEO, based on the *Baker et al.* [1990] analysis. This work has formed the basis
398 for the Relativistic Electron Forecast Model (REFM) that has, for many years, been operational
399 at the Space Weather Prediction Center of NOAA in Boulder, Colorado (www.swpc.noaa.gov/
400 products/relativistic-electron-forecast-model).
401 As was noted previously, however, statistical studies of the relationship of solar wind speed
402 and total electron radiation belt content [*Baker et al.*, 2004] or GEO relativistic electron fluxes
403 [*Reeves et al.*, 2011; *Li et al.*, 2011] show that there can be very high radiation belt particle
404 fluxes even when concurrent solar wind speeds are quite low. Thus, there is tremendous scatter
405 in the data. What is demonstrably true is that relativistic electron fluxes in the outer Van Allen
406 belt only seldom are low when the solar wind speed is high; thus, a triangular distribution pattern
407 is found for the scatter plots of flux and its moments (number and energy density and
408 temperature) versus solar wind speed [*Baker et al.*, 2004; *Reeves et al.*, 2011; *Hartley et al.*,
409 2014]: High fluxes at low solar wind speeds are common, but there are few cases of low fluxes
410 (or low number and energy densities) at high solar wind speeds.

411 The work presented here shows that, at least some of the time, the above pattern is violated.
412 When the IMF is northward during and after a high-speed solar wind stream period, the outer
413 zone electron flux level can be quite low throughout the stream period. From the statistical
414 studies cited above, such events must be relatively rare. In most cases of high-speed streams,
415 there must be enough southward IMF to produce substorm injections of source and seed
416 electrons.

417 The results presented in this paper make it quite clear that the radiation belt accelerator is a
418 rather finely tuned "machine". If the IMF does not have a southward component during an
419 episode of high solar wind flow speed, then magnetospheric substorm activity does not occur.
420 Without substorms, there is no injection of hot plasma and energetic electrons into the region $5 \leq$
421 $L \leq 7$. Without the source particles (up to tens of keV energy) the lower band chorus waves are
422 not produced (amplified). Without chorus waves – even if there are residual seed population
423 electrons – there is not an effective acceleration event for multi-MeV electrons in the outer zone.
424 Moreover, not all substorms are capable of initiating this process. For example, the particle
425 injections on 16 September, mentioned earlier as ending a three-day period of decreasing fluxes,
426 injected a source population over a limited L-range and lacked a substantially enhanced seed
427 population; the injections were only prominent in the 30-100 keV fluxes at GOES-13 (Figure 2)
428 and did not extend inwards of L=5.5-6 (Figure 4). In contrast, the injections on 22 September
429 had a large >100 keV component at GOES-13 (Figure 2) and were associated with a large
430 increase in MagEIS 30 keV fluxes nearly to L=4 (Figure 4) and with an increase in E>2 MeV
431 fluxes above the GOES instrument backgrounds.

432 This paper has also addressed to some extent the questions surrounding the role of ULF
433 waves in the acceleration, transport, and loss of relativistic electrons in the outer zone. As shown,

for example, by *Rostoker et al.* [1998], ULF wave power enhancements often are associated with relativistic electron outer belt flux increases. In this paper, we have confirmed such an association throughout the outer radiation zone. It appears that ULF waves play two key roles: 1) Enhanced outward diffusion of electrons toward the magnetopause to help drive radiation belt depletion; and 2) Enhanced inward radial diffusion of mildly relativistic electrons (1-2 MeV) to pump up electrons to multi-MeV energies in the trailing part of high-speed solar wind streams. However, the full significance of ULF involvement in the process detailed here is not entirely clear, and further study is planned to evaluate the role of ULF waves in this time period, and other analagous events.

Acknowledgements

The research presented here was supported by RBSP-ECT funding through JHU/APL contract 967399 (under prime NASA contract NAS5-01072). All data used in this paper is currently available via CDAweb (http://cdaweb.gsfc.nasa.gov/) or through the individual Van Allen Probes instrument suite webpages. We wish to thank S. Claudepierre of the MagEIS team for providing data for this study prior to its public release.

References

Baker, D. N., P. R. Higbie, R. D. Belian, and E. W. Hones, Jr., Do Jovian electrons influence the terrestrial outer radiation zone?, Geophys. Res. Letters, 6, 531, 1979.

Baker, D. N., J. B. Blake, R. W. Klebesadel, and P. R. Higbie, Highly relativistic electrons in the Earth's outer magnetosphere, I. Lifetimes and temporal history 1979-1984, J. Geophys. Res., 91, 4265, 1986.

Baker, D. N., R. L. McPherron, T. E. Cayton, and R. W. Klebesadel, Linear prediction filter analysis of relativistic electron properties at 6.6 R_E, J. Geophys. Res., 95, 15133, 1990.

Baker, D. N., T. I. Pulkkinen, V. Angelopoulos, W. Baumjohann, and R. L. McPherron, The neutral line model of substorms: Past results and present view, J. Geophys. Res., 101, 12,995-13,010, 1996.

Baker, D. N., X. Li, N. Turner, J. H. Allen, J. B. Blake, R. B. Sheldon, H. E. Spence, R. D. Belian, G. D. Reeves, S. G. Kanekal, B. Klecker, R. P. Lepping, K. Ogilvie, R. A. Mewaldt, T. Onsager, H. J. Singer, and G. Rostoker, Recurrent geomagnetic storms and relativistic electron enhancements in the outer magnetosphere: ISTP coordinated measurements, J. Geophys. Res., 102, 14,141-14,148, 1997a.

Baker, D. N., S. G. Kanekal, and J. B. Blake, Characterizing the Earth’s Outer Van Allen zone using the Radiation Belt Content (RBC) Index, Space Weather, 2, S02003, doi:10.1029/2003SW000026, 2004.

Baker, D. N., et al., The Relativistic Electron-Proton Telescope (REPT) Instrument on board the Radiation Belt Storm Probes (RBSP) Spacecraft: Characterization of Earth’s radiation belt high-energy particle populations, Space Science Rev., doi:10.1007/s11214-012-9950-9, 2012.

475 Baker, D. N., et al., A long-lived relativistic electron storage ring embedded within the Earth's
476 outer Van Allen Radiation Zone, Science, 340, #6129, 186-190, doi:10.1126/
477 science.1233518, 2013. Published online February 28, 2013.
478 Baker, D. N., A. N. Jaynes, V. C. Hoxie, R. M. Thorne, J. C. Foster, X. Li, J. F. Fennell, J. R.
479 Wygant, S. G. Kanekal, P. J. Erickson, W. Kurth, W. Li, Q. Ma, Q. Schiller, L. Blum, D. M.
480 Malaspina, A. Gerrard, and L. J. Lanzerotti, An impenetrable barrier to ultra-relativistic
481 electrons in the Van Allen Radiation Belt, Nature, 515, 531-534, doi:10.1038/nature13956,
482 2014a.
483 Baker D. N., A. N. Jaynes, X. Li, M. G. Henderson, S. G. Kanekal, G. D. Reeves, H. E. Spence,
484 S. G. Claudepierre, J. F. Fennell, M. K. Hudson, R. M. Thorne, J. C. Foster, P. J. Erickson,
485 D. M. Malaspina, J. R. Wygant, A. Boyd, C. A. Kletzing, A. Drozdov, and Y. Y. Shprits,
486 Gradual diffusion and punctuated phase space density enhancements of highly relativistic
487 electrons: Van Allen Probes Observations, Geophys. Res. Lett., 41, #5, 1351-1358, 16 March
488 2014, doi:10.1002/2013GL058942, published online 4 March 2014, 2014b.
489 Blake, J. B., D. N. Baker, N. Turner, K. W. Ogilvie, and R. P. Lepping, Correlation of changes in
490 the outer-zone relativistic electron population with upstream solar wind and magnetic field
491 measurements, Geophys. Res. Lett., 24, 927-929, 1997.
492 Blake, J. B., et al., The Magnetic Electron Ion Spectrometer (MagEIS) Instruments aboard the
493 Radiation Belt Storm Probes (RBSP) Spacecraft, Space Sci. Rev., doi:10.1007s/11214-013-
494 9991-8, 2013.
495 Boyd, A. J., H. E. Spence, S. G. Claudepierre, J. F. Fennell, J. B. Blake, D. N. Baker, G. D.
496 Reeves, D. L. Turner, and H. O Funsten, Quantifying the radiation belt seed population in the

497 17 March 2013 electron acceleration event, *Geophys. Res. Lett.*, doi:10.1002/2014GL059626,
498 2014.
499 Chen, Y., R. H. W. Friedel, and G. D. Reeves (2006), Phase space density distributions of
500 energetic electrons in the outer radiation belt during two Geospace Environment Modeling
501 Inner Magnetosphere/Storms selected storms, J. Geophys. Res., 111, A11S04,
502 doi:10.1029/2006JA011703.
503 Claudepierre, S. G., S. R. Elkington, and M. Wiltberger, Solar wind driving of magnetospheric
504 ULF waves: Pulsations driven by velocity shear at the magnetopause, J. Geophys. Res., 113,
505 A05218, doi:10.1029/2007JA012890, 2008.
506 Elkington, S. R., A. A. Chan, and M. Wiltberger, M., Global Structure of ULF Waves During the
507 24–26 September 1998 Geomagnetic Storm, in Dynamics of the Earth's Radiation Belts and
508 Inner Magnetosphere (D. Summers, I. R. Mann, D. N. Baker and M. Schulz, eds.), American
509 Geophysical Union, Washington, D. C.. doi: 10.1029/2012GM001348, 2012.
510 Fennell, J. F., S. G. Claudepierre, J. B. Blake, T. P. O'Brien, J. H. Clemmons, D. N. Baker, H. E.
511 Spence, and G. D. Reeves, Van Allen Probes show the inner radiation zone contains no MeV
512 electrons: ECT/MagEIS data, Geophys. Res. Lett., DOI: 10.1002/2014GL062874, 2015.
513 Foster, J.C., P.J. Erickson, D.N. Baker, S.G. Claudepierre, C.A. Kletzing, W. Kurth, G.D.
514 Reeves, S.A. Thaller, H.E. Spence, Y.Y. Shprits, and J.R. Wygant, Prompt energization of
515 relativistic and highly relativistic electrons during substorm intervals: Van Allen Probes
516 Observation, Geophys. Res. Lett., 41, 20-25, doi: 10.1002/2013GL058438, 2014.
517 Funsten, H. O., R. M. Skoug, A. A. Guthrie, E. A. MacDonald, J. R. Baldonado, R. H. Harper,
518 K. C. Henderson, K. H. Kihara, J. E. Lake, B. A. Larsen, A. D. Puckett, V. J. Vigil, R. H.
519 W. Friedel, M. G. Henderson, J. T. Niehof, G. D. Reeves, and M. F. Thomsen

(2013), Helium, Oxygen, Proton, and Electron (HOPE) Mass Spectrometer for the Radiation Belt Storm Probes Mission, Space Science Reviews, doi:10.1007/s11214-013-9968-7.

Green, J.C., T.G. Onsager, T.P. O'Brien, and D.N. Baker, Testing loss mechanisms capable of rapidly depleting relativistic electron flux in the Earth's outer radiation belt, J. Geophys. Res., 109, A12211, doi:10.1029/2004JA010579, 2004.

Green, J. C., and M. G. Kivelson (2004b), Relativistic electrons in the outer radiation belt: Differentiating between acceleration mechanisms, J. Geophys. Res., 109, A03213, doi:10.1029/2003JA010153.

Hajra, R., et al., Relativistic (E>0.6, >2.0, and >4.0 MeV) electron acceleration at geosynchronous orbit during high-intensity, long duration, continuous AE activity (HILDCAA) events, ApJ, 799 39, doi:10.1088/0004-637X/799/1/39, 2015.

Hanser, F.A., EPS/HEPAD calibration and data handbook, Tech. Rep. GOESN-ENG-048D, Assurance Technology Corporation, Carlisle, Mass., 2011.

Hartley, D.P., M.H. Denton, J C. Green, T.G. Onsager, J.V. Rodriguez, and H.J. Singer, Case studies of the impact of high-speed solar wind streams on the electron radiation belt at geosynchronous orbit: Flux, magnetic field, and phase space density, J. Geophys. Res. Space Physics, 118, 6964–6979, doi:10.1002/2013JA018923, 2013.

Hartley, D.P., M.H. Denton, and J.V. Rodriguez, Electron number density, temperature, and energy density at GEO and links to the solar wind: A simple predictive capability, J. Geophys. Res. Space Physics, 119, 4556-4571, doi: 10.1002/2014JA019779, 2014.

Hietala, H., E. K. J. Kilpua, D. L. Turner, and V. Angelopoulos (2014), Depleting effects of ICME-driven sheath regions on the outer electron radiation belt, Geophys. Res. Lett., 41, 2258–2265, doi:10.1002/2014GL059551.

543 Horne, R. B., R. M. Thorne, S. A. Glauert, J. M. Albert, N. P. Meredith, and R. R. Anderson
544 (2005), Timescale for radiation belt electron acceleration by whistler mode chorus waves,
545 J. Geophys. Res., 110, A03225, doi:10.1029/2004JA010811.

546 Hudson, M.K., S.R. Elkington, J.G. Lyon, V.A. Marchenko, I. Roth, M. Temerin, J.B. Blake, M.S.
547 Gussenhoven and J.R. Wygant, Simulations of radiation belt formation during storm sudden
548 commencements, J. Geophys. Res.,102, 14087, doi: 10.1029/97JA03995, 1997.

549 Hudson, Mary K., Brian T. Kress, Hans-R. Mueller, Jordan A. Zastrow, J. Bernard Blake,
550 Relationship of the Van Allen radiation belts to solar wind drivers, Journal of
551 Atmospheric and Solar-Terrestrial Physics, 70 (5), 2008, 708-729,
552 doi:10.1016/j.jastp.2007.11.003.

553 Kanekal, S. G., D. N. Baker, J. B. Blake, B. Klecker, R. A. Mewaldt, and G. M. Mason,
554 Magnetospheric response to magnetic cloud (coronal mass ejection) events: Relativistic
555 electron observations from SAMPEX and Polar, J. Geophys. Res., 104, #A11, 24885-24894,
556 doi: 10.1029/1999JA900239, 1999.

557 Kletzing, C.A., et al., The Electric and Magnetic Field Instrument and Suite and Integrated
558 Science (EMFISIS) on RBSP, Space Sci. Rev., 179, 127-181, 2013.

559 Li, W., B. Ni, R. M. Thorne, J. Bortnik, J. C. Green, C. A. Kletzing, W. S. Kurth, and G. B.
560 Hospodarsky, Constructing the global distribution of chorus wave intensity using
561 measurements of electrons by the POES satellites and waves by the Van Allen Probes,
562 Geophys. Res. Lett., 40, 4526–4532, doi:10.1002/grl.50920, 2013.

563 Li, W., R. M. Thorne, Q. Ma, B. Ni, J. Bortnik, D. N. Baker, H. E. Spence, G. D. Reeves, S. G.
564 Kanekal, J. C. Green, C. A. Kletzing, W. S. Kurth, G. B. Hospodarsky, J. B. Blake, J. F.

565 Fennell, and S. G. Claudepierre, Radiation belt electron acceleration by chorus waves during
566 the 17 March 2013 storm, J. Geophys. Res., 119, #6, 4681-4693,
567 doi:10.1002/2014JA019945, 2014.

568 Li, X., M. Temerin, D.N. Baker, and G.D. Reeves, Behavior of MeV electrons at
569 geosynchronous orbit during last two solar cycles, J. Geophys. Res., 116, A11207,
570 doi:10.1029/2011JA016934, 2011.

571 Li, X., R. S. Selesnick, D. N. Baker, A. N. Jaynes, S. G. Kanekal, Q. G. Schiller, and L. W.
572 Blum, Upper limit on the inner radiation belt MeV electron intensity**,**
573 J. Geophys. Res. Space Physics, 120, doi: 10.1002/2014JA020777, 2015.

574 Luo, B., X. Li, M. Temerin, and S. Liu, Prediction of the *AU*, *AL*, and *AE* indices using solar
575 wind parameters, J. Geophys. Res. Space Physics, 118, doi:10.1002/2013JA019188, 2013.

576 McIlwain, C.E., Magnetic coordinates, Space Science Reviews, 5, 585-598, 1966.

577 McPherron, R.L., C.T. Russell, and M.P. Aubry, Satellite studies of magnetospheric substorms
578 on August 15, 1968, 9, Phenomenological model for substorms, J. Geophys. Res., 78, 3131,
579 1973.

580 Miyoshi, Y., and R. Kataoka, Flux enhancement of the outer radiation belt electrons after the
581 arrival of stream interaction regions, J. Geophys. Res., 113, A03209,
582 doi:10.1029/2007JA012506, 2008.

583 Onsager, T.G., R. Grubb, J. Kunches, L. Matheson, D. Speich, R. Zwickl, and H. Sauer,
584 Operational uses of the GOES energetic particle detectors, in GOES-8 and Beyond: 7–9
585 August 1996, Denver, Colorado, edited by E. R. Washwell, Proc. SPIE Int. Soc. Opt. Eng.,
586 2812, 281, 1996.

587 Onsager, T.G., G. Rostoker, H.-J. Kim, G.D. Reeves, T. Obara, H.J. Singer and C. Smithtro,
588 Radiation belt electron flux dropouts: Local time, radial, and particle-energy dependence, J.
589 Geophys. Res., 107, #A11, doi:10.1029/2001JA000187, 2002.
590 Onsager, T.G., J.C. Green, G.D. Reeves, and H.J. Singer, Solar wind and magnetospheric
591 conditions leading to the abrupt loss of outer radiation belt electrons, J. Geophys. Res., 112,
592 A01202, doi:10.1029/2006JA011708, 2007.
593 Paulikas, G.A. and J.B. Blake, In: Effects of the solar wind on magnetospheric dynamics:
594 Energetic electrons at the synchronous orbit, American Geophysical Union, Washington D.C.
595 21: 5-2. doi: 10.1029/GM021p0180, 1979.
596 Reeves, G.D., K.L. McAdams, R.H.W. Friedel, and T.P. O'Brien, Acceleration and loss of
597 relativistic electrons during geomagnetic storms, Geophys. Res. Lett., 30, #10, 36-1, CiteID
598 1529, doi:10.1029/2002GL016513, 2003a.
599 Reeves, G.D., et al., On the relationship between relativistic electron flux and solar wind
600 velocity: Paulikas and Blake revisited, J. Geophys. Res., 116, #A2,
601 doi:10.1029/2010JA015735, 2011.
602 Reeves, G.D., H. Spence, M. Henderson, S. Morley, R.H.W. Friedel, H. Funsten, D.N. Baker, S.
603 Kanekal, J. Blake, J. Fennell, S. Claudepierre, R. Thorne, D. Turner, C. Kletzing, W. Kurth,
604 B. Larsen, and J. Niehof, Electron acceleration in the heart of the Van Allen Radiation Belts,
605 Science, Vol. 341, #6149, 991-994, doi: 10.1126/science.1237743, 2013.
606 Rodriguez, J. V. (2014), GOES EPEAD Science-Quality Electron Fluxes Algorithm Theoretical
607 Basis Document, NOAA National Geophysical Data Center

608 Rostoker, G., S. Skone, and D.N. Baker, On the origin of relativistic electrons in the
609 magnetosphere associated with some geomagnetic storms, Geophys. Res. Lett., 25, 3701-
610 3704, 1998.
611 Rufenach, C.L, R.F. Martin, Jr., and H.H. Sauer, A study of geosynchronous magnetopause
612 crossings, J. Geophys. Res., 94(A11), 15125-15134, doi:10.1029/JA094iA11p15125, 1989.
613 Sergeev, V.A., et al., Event study combining magnetospheric and ionospheric perspectives of the
614 substorm current wedge modeling, J. Geophys. Res., 119, 9714-9728,
615 doi:10.1029/2014JA020522, 2015.
616 Shue, J.-H., et al. (1998), Magnetopause location under extreme solar wind conditions, J.
617 Geophys. Res., 103(A8), 17691–17700, doi:10.1029/98JA01103.

618 Singer, H. J., L. Matheson, R. Grubb, A. Newman, and S. D. Bouwer, Monitoring space weather
619 with GOES magnetometers, SPIE Proc., 2812, 1996.
620 Spence, H. E., et al., Science Goals and Overview of the Energetic Particle, Composition, and
621 Thermal Plasma (ECT) Suite on NASA's Radiation Belt Storm Probes (RBSP) Mission,
622 *Space Sci. Rev.*, DOI: 10.1007/s11214-013-0007-5, 2013.
623 Summers, D., C. Ma, N. P. Meredith, R. B. Horne, R. M. Thorne, D. Heynderickx, and R. R.
624 Anderson, Model of the energization of outer-zone electrons by whistler-mode chorus
625 during the October 9, 1990 geomagnetic storm,Geophys. Res. Lett., 29(24), 2174,
626 doi:10.1029/2002GL016039, 2002.

627 Summers, D., C. Ma, and T. Mukai (2004), Competition between acceleration and loss
628 mechanisms of relativistic electrons during geomagnetic storms, J. Geophys. Res., 109,
629 A04221, doi:10.1029/2004JA010437.

630 Summers, D., R. Tang, Y. Omura, Linear and nonlinear growth of magnetospheric whistler mode
631 waves, Introduction, AGU Geophys. Monograph Series, 199, doi:10.1029/2012GM001298,
632 2012.
633 Temerin, M., and X. Li, *Dst* model for 1995–2002, J. Geophys. Res., 111, A04221, doi:10.1029/
634 2005JA011257, 2006.
635 Thorne, R.M., W. Li, B. Ni, Q. Ma, J. Bortnik, D.N. Baker, H.E. Spence, G.D. Reeves, M.G.
636 Henderson, C.A. Kletzing, W.S. Kurth, G.B. Hospodarsky, D. Turner, and V. Angelopoulos,
637 Evolution and slow decay of an unusual narrow ring of relativistic electrons near L~ 3.2
638 following the September 2012 magnetic storm, Geophys. Res. Lett., 40, 3507,
639 doiP10.1002/grl.50627, 2013a.
640 Thorne, R.M., et al., Rapid local acceleration of relativistic radiation belt electrons by
641 magnetospheric chorus, Nature, 504, 411–414, doi:10.1038/nature12889, Published online 18
642 December 2013b.
643 Tsurutani, B.T., W.D. Gonzalez, A.L.C. Gonzalez, F. Tang, J.K. Arballo, and M. Okada,
644 Interplanetary origin of geomagnetic activity in the declining phase of the solar cycle, J.
645 Geophys. Res., 100, 21717–21733, 1995.
646 Tu, W., G.S. Cunningham, Y. Chen, S.K. Morley, G.D. Reeves, J.B. Blake, D.N. Baker, and H.
647 Spence, Event-specific chorus wave and electron seed population models in DREAM3D
648 using the Van Allen Probes, Geophys. Res. Lett., 41, #5, 1359-1366,
649 doi:10.1002/2013gl058819, 2014.
650 Turner, D.L., et al., Explaining sudden losses of outer radiation belt electrons during
651 geomagnetic storms, Nat. Phys. 8, 208-212, doi:10.1038/nphys2185, 2012.

652 Wilken, B., C. K. Goertz, D. N. Baker, P. R. Higbie, and T. A. Fritz, The SSC on July 29, 1977
653 and its propagation within the magnetosphere, J. Geophys. Res., 87, 5901, 1982.
654
655

Figures

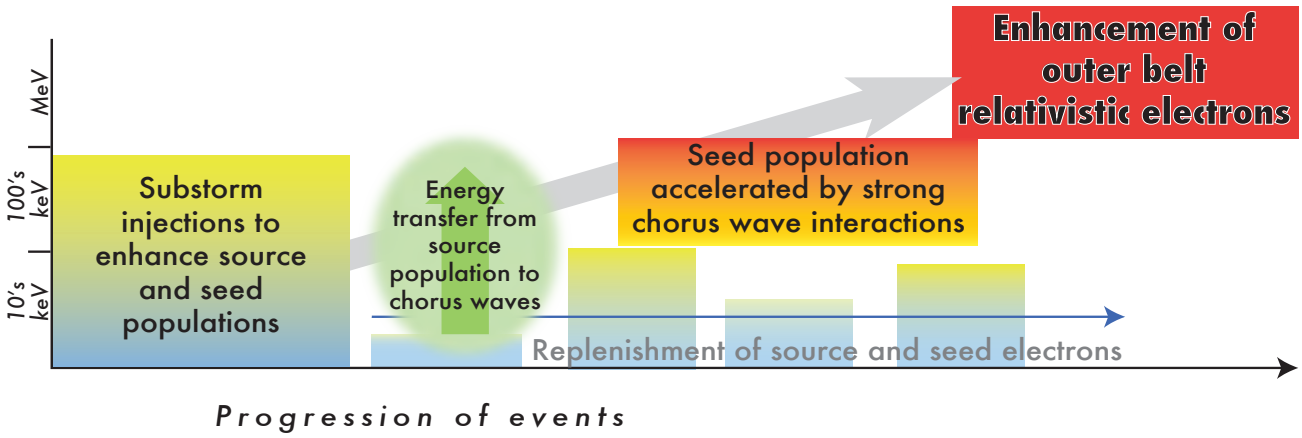

Fig 1: Schematic of the ideal setup and sequence for strong enhancement of outer belt electrons >1 MeV.

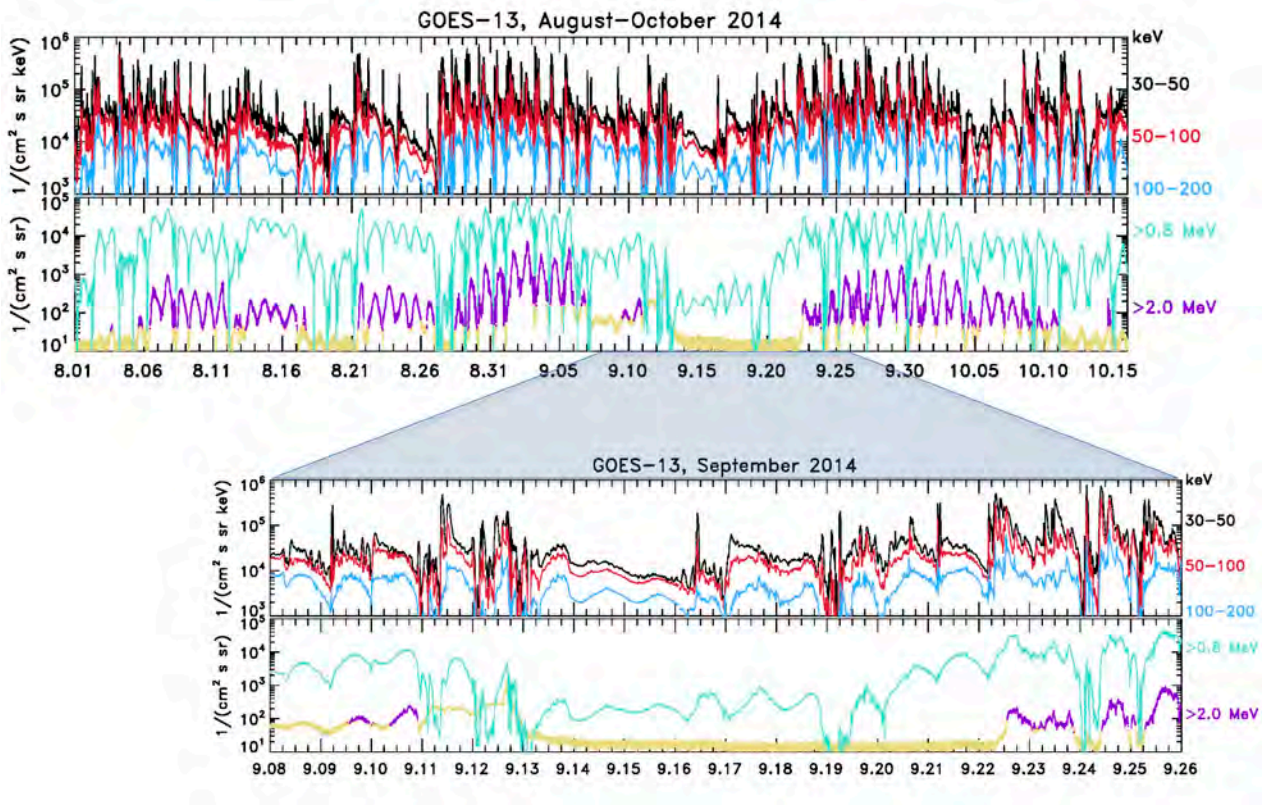

664

665 Fig 2: Overview of GOES observations over range of energies: Aug 01-Oct 15, and Sep 08-26
666 for inset. Light brown traces indicate the fluxes for times when the background count rate is at
667 least 30% of the observed count rate. Sept 11-13 is during a weak SEP event, and Sept 13-22 is
668 when the >2 MeV electrons are below the galactic cosmic ray instrument backgrounds.

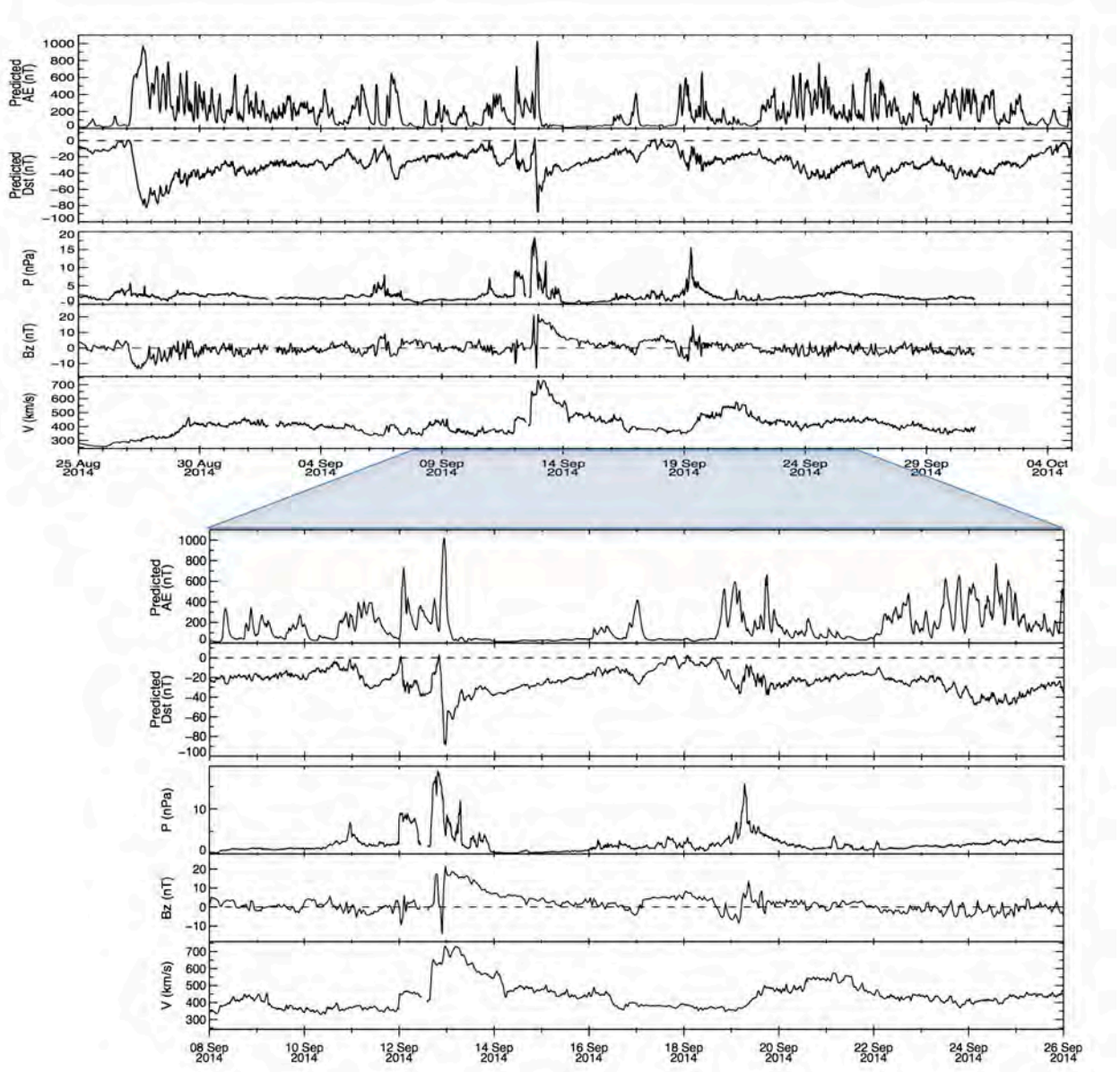

669

670 Fig 3: Predicted AE (Luo et al., 2013) and Dst (Temerin and Li, 2006), with solar wind pressure,

671 Bz and velocity: Aug 25-Oct 04, and Sep 08-26 for inset.

672

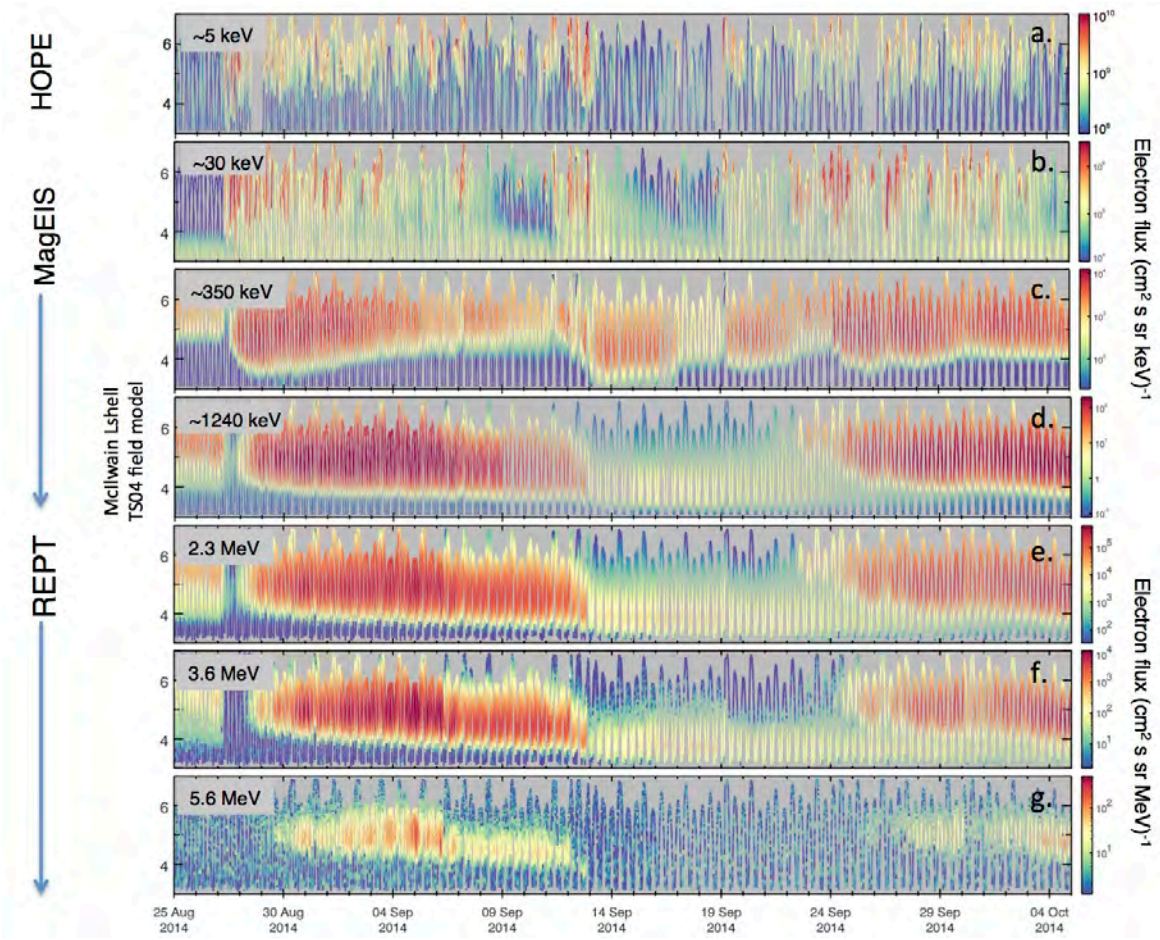

673

674 Fig 4: Spin-averaged flux over HOPE, MagEIS and REPT energy range: Aug 25-Oct 04.

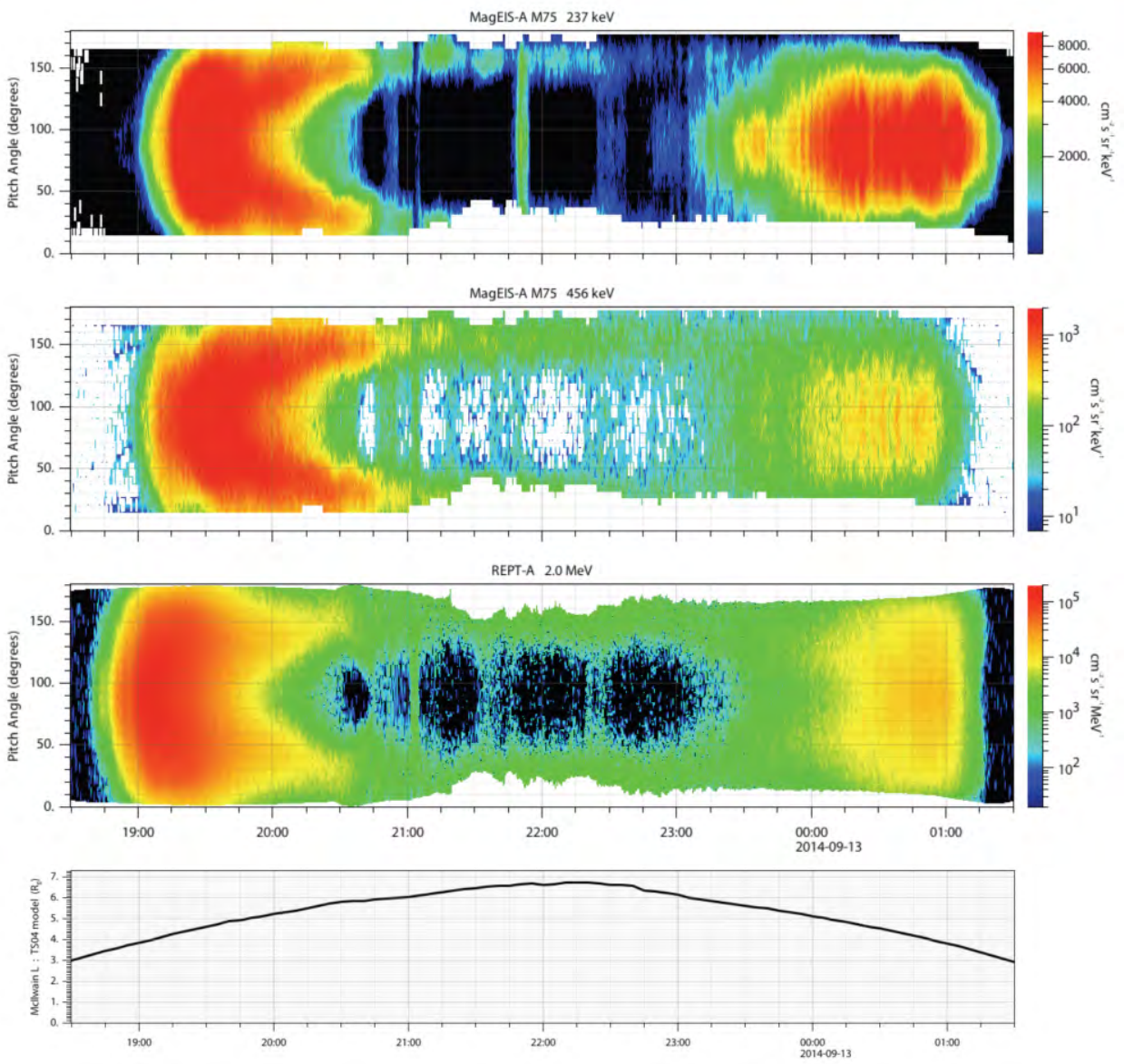

675

676 Fig 5: Pitch angle distribution spectrograms for selected REPT and MagEIS energies for the

677 period of magnetopause shadowing loss during the main phase of the Sept 12th storm (top three

678 panels) and McIlwain L-shell value calculated in the TS04 magnetic field model (bottom panel).

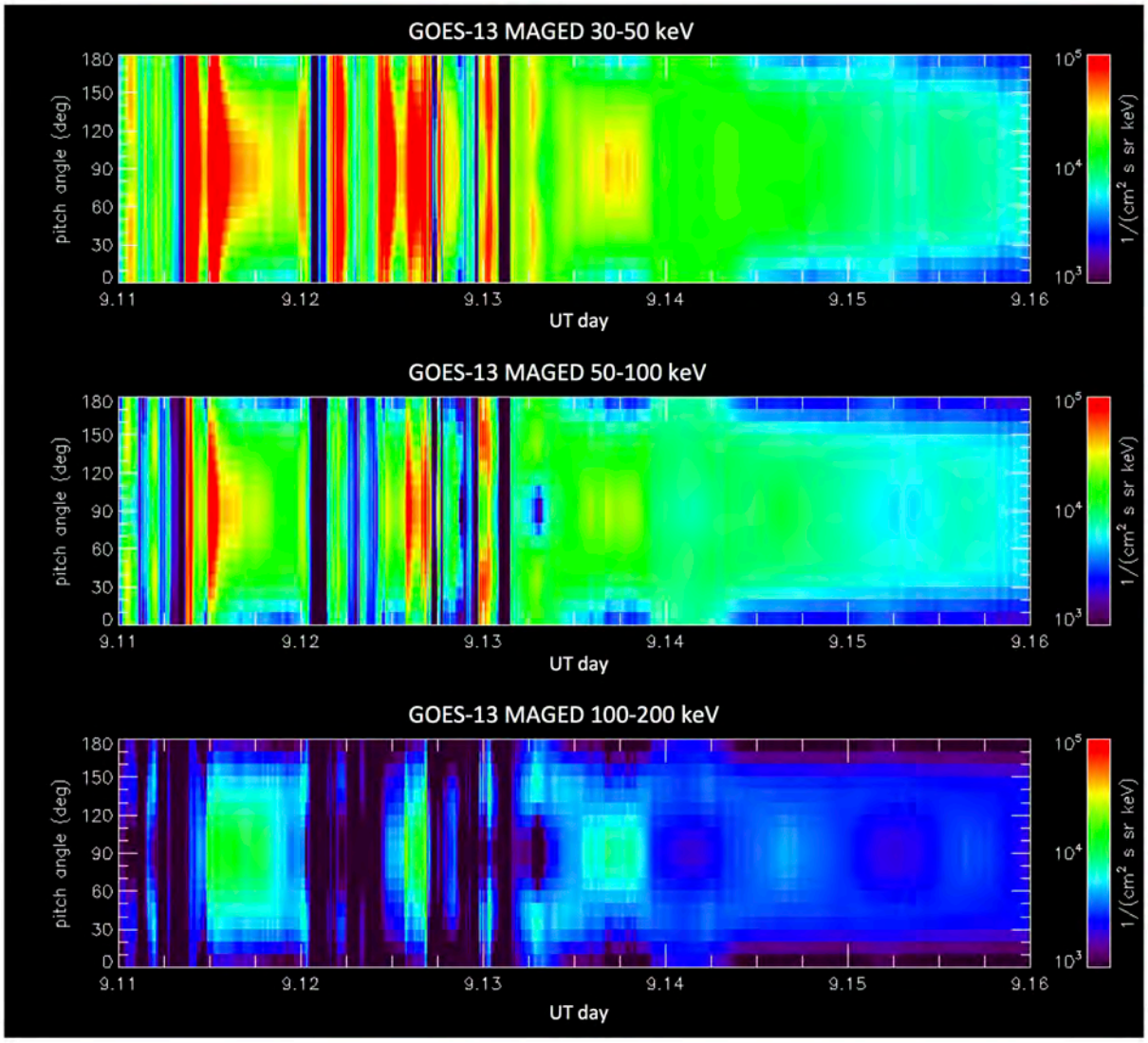

679

680 Fig 6: Pitch angle distribution spectrograms for selected GOES-13 energies: Sep 11-15.

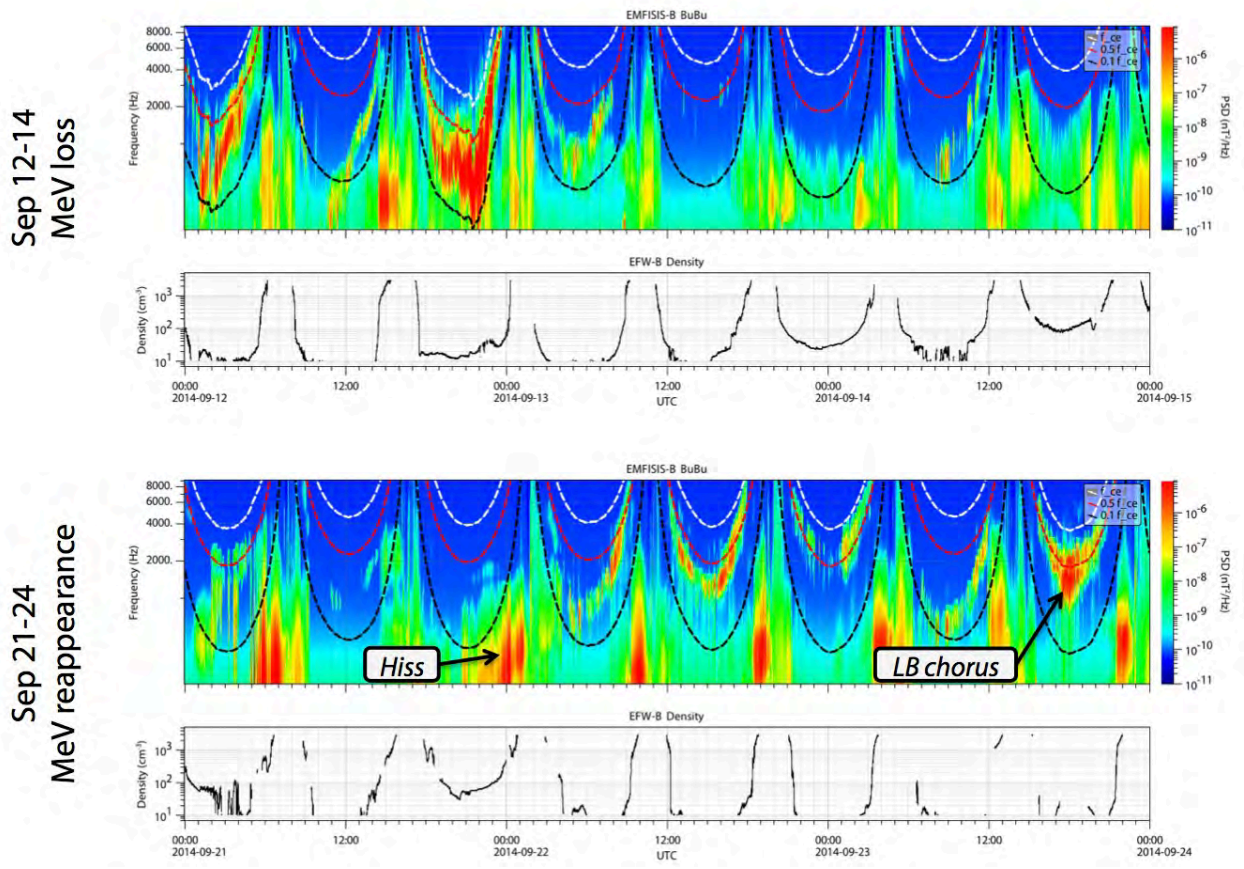

Fig 7: Chorus wave power spectral density spectrograms from EMFISIS-B magnetic field measurements and electron density derived from spacecraft potential during September 12 storm (top panels) and recovery of relativistic outer belt (bottom panels); lines denote fractions of the electron gyro frequency at 0.1 f_ce (black), 0.5 f_ce (red) and 1.0 f_ce (white) in order to bound the lower- and upper-band chorus observations.

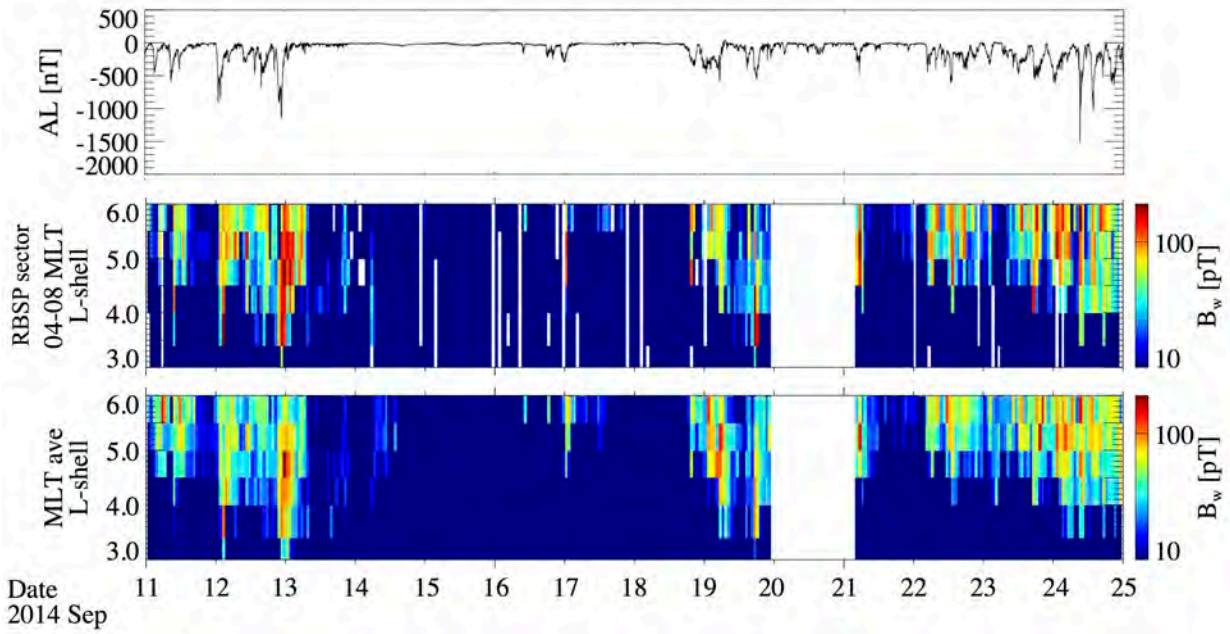

687

688 Fig 8: Inferred chorus wave amplitudes by using a proxy based on POES electron precipitation
689 measurements (30-100 keV). (Top) AL Index. (Middle) Evolution of inferred chorus wave
690 amplitude averaged over 04-08 MLT, where the apogees of the Van Allen Probes were located.
691 (Bottom) Evolution of inferred chorus wave amplitude averaged over all MLTs.

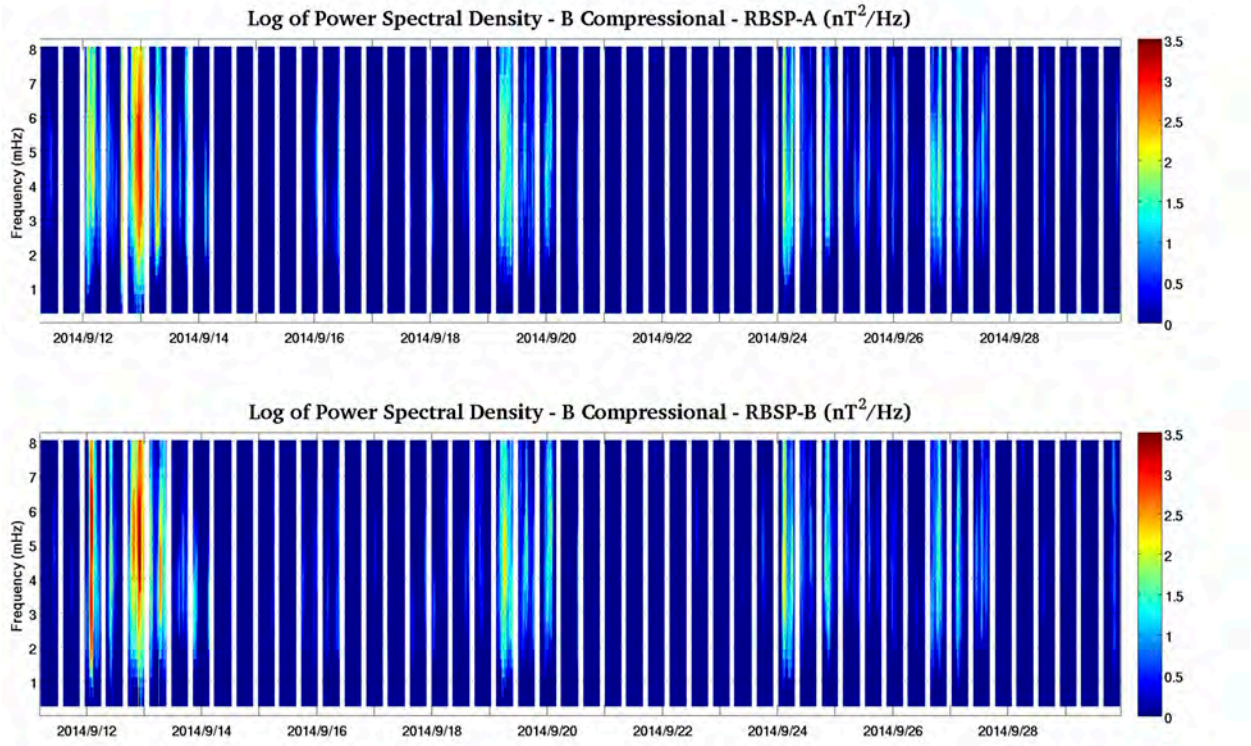

692

693 Fig 9: ULF power spectral density overview during the Sept storm through to the recovery of the

694 MeV: 11-30 September.

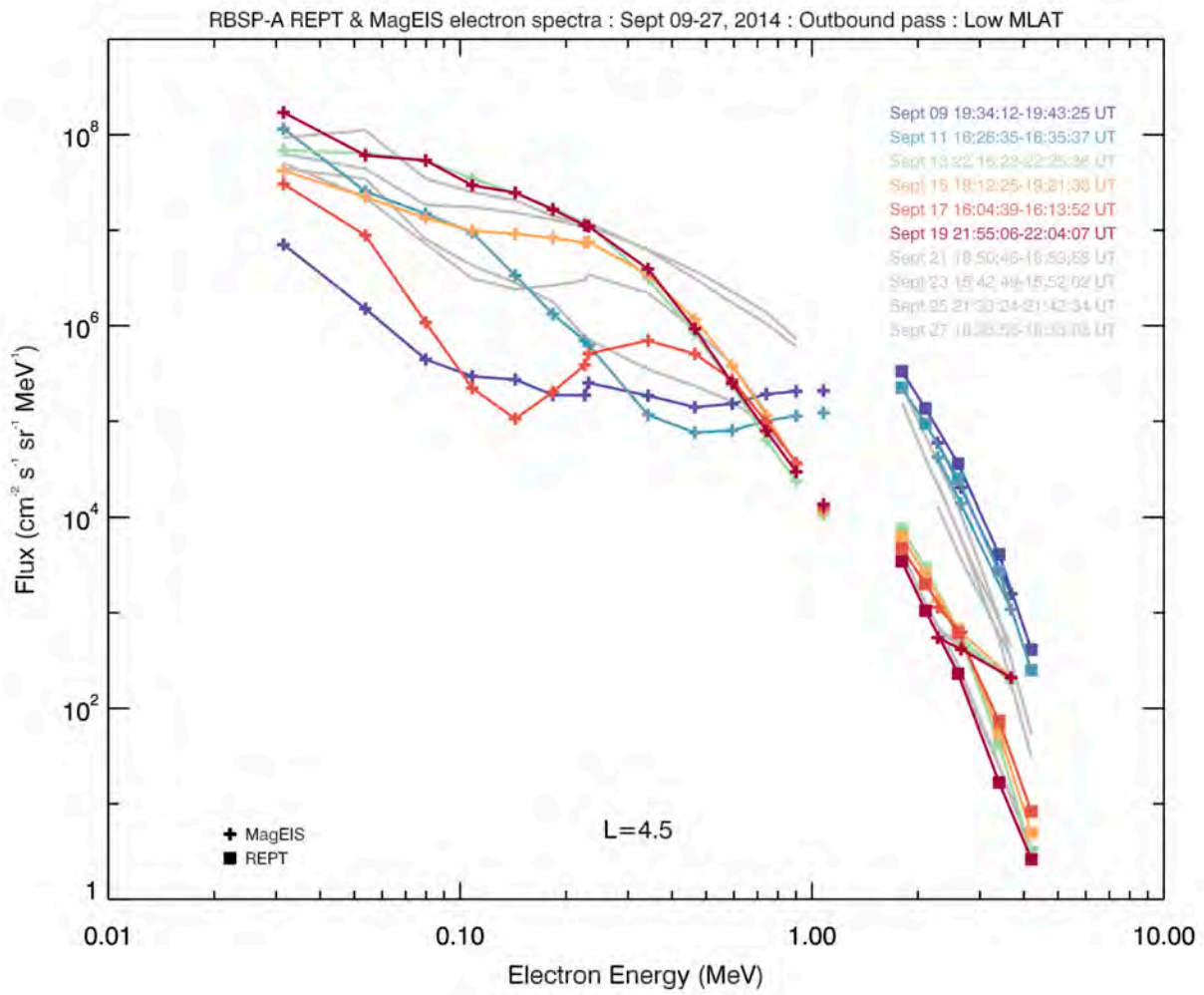

695

696 Fig 10: Evolution of energy spectrum across MagEIS and REPT energies: Sep 09-27. The gap in

697 the energy spectra from >1 MeV to ~2.5 MeV is due to missing MagEIS data channels over this

698 full event period. All spectra are taken from outbound passes at MLAT ≤ ~5°.

699

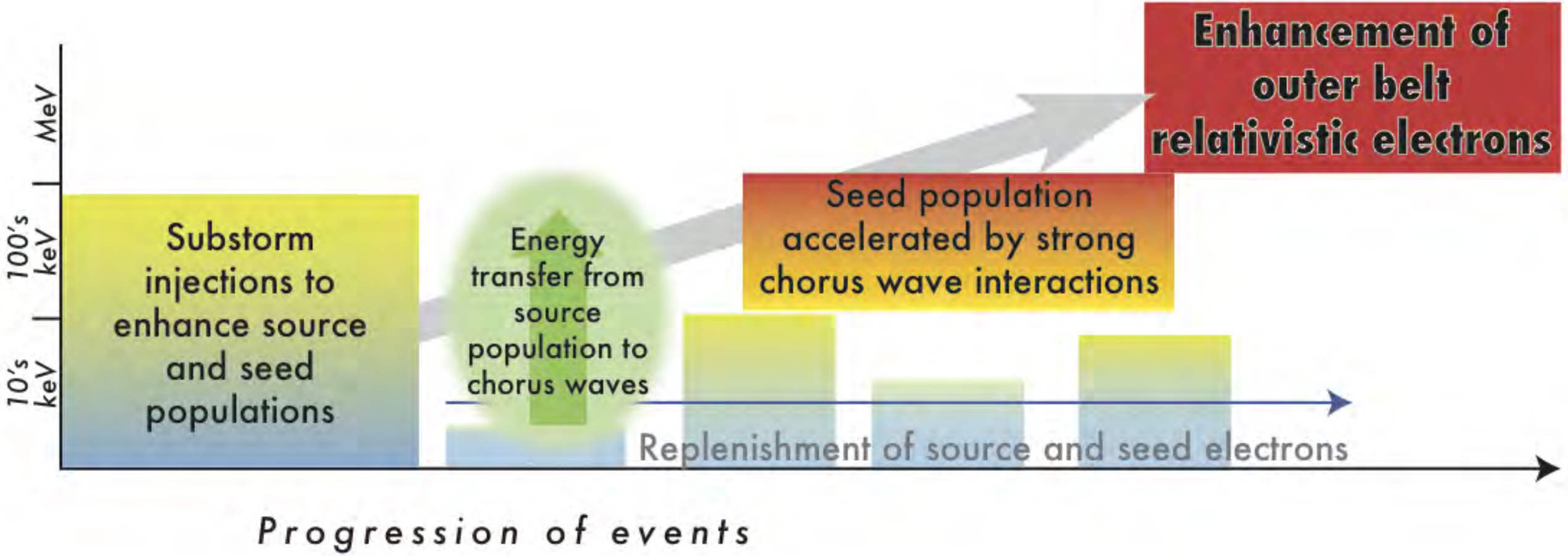
Enhancement of outer belt relativistic electrons
Seed population accelerated by strong chorus wave interactions
Energy transfer from source population to chorus waves
Substorm injections to enhance source and seed populations
MeV
100's keV
10's keV
Replenishment of source and seed electrons
Progression of events

GOES−13, August−October 2014

1/(cm² s sr keV)

keV

30−50

50−100

100−200

1/(cm² s sr)

>0.8 MeV

>2.0 MeV

8.01 8.06 8.11 8.16 8.21 8.26 8.31 9.05 9.10 9.15 9.20 9.25 9.30 10.05 10.10 10.15

GOES−13, September 2014

9.08 9.09 9.10 9.11 9.12 9.13 9.14 9.15 9.16 9.17 9.18 9.19 9.20 9.21 9.22 9.23 9.24 9.25 9.26

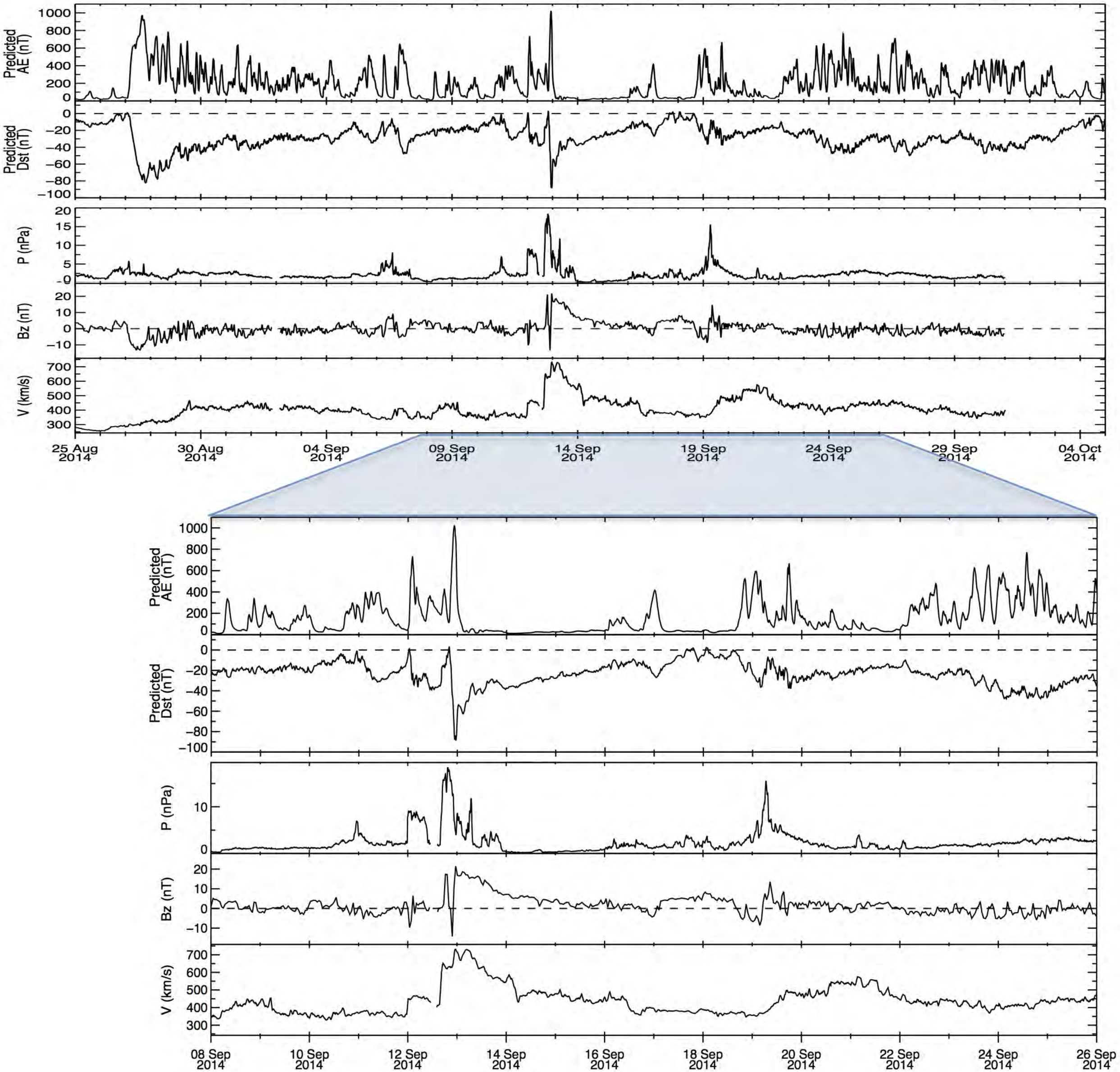
Predicted AE (nT)
1000
800
600
400
200
0
Predicted Dst (nT)
0
−20
−40
−60
−80
−100
P (nPa)
20
15
10
5
-0
Bz (nT)
20
10
0
−10
V (km/s)
700
600
500
400
300
25 Aug 2014
30 Aug 2014
04 Sep 2014
09 Sep 2014
14 Sep 2014
19 Sep 2014
24 Sep 2014
29 Sep 2014
04 Oct 2014
Predicted AE (nT)
1000
800
600
400
200
0
Predicted Dst (nT)
0
−20
−40
−60
−80
−100
P (nPa)
10
0
Bz (nT)
20
10
0
−10
V (km/s)
700
600
500
400
300
08 Sep 2014
10 Sep 2014
12 Sep 2014
14 Sep 2014
16 Sep 2014
18 Sep 2014
20 Sep 2014
22 Sep 2014
24 Sep 2014
26 Sep 2014

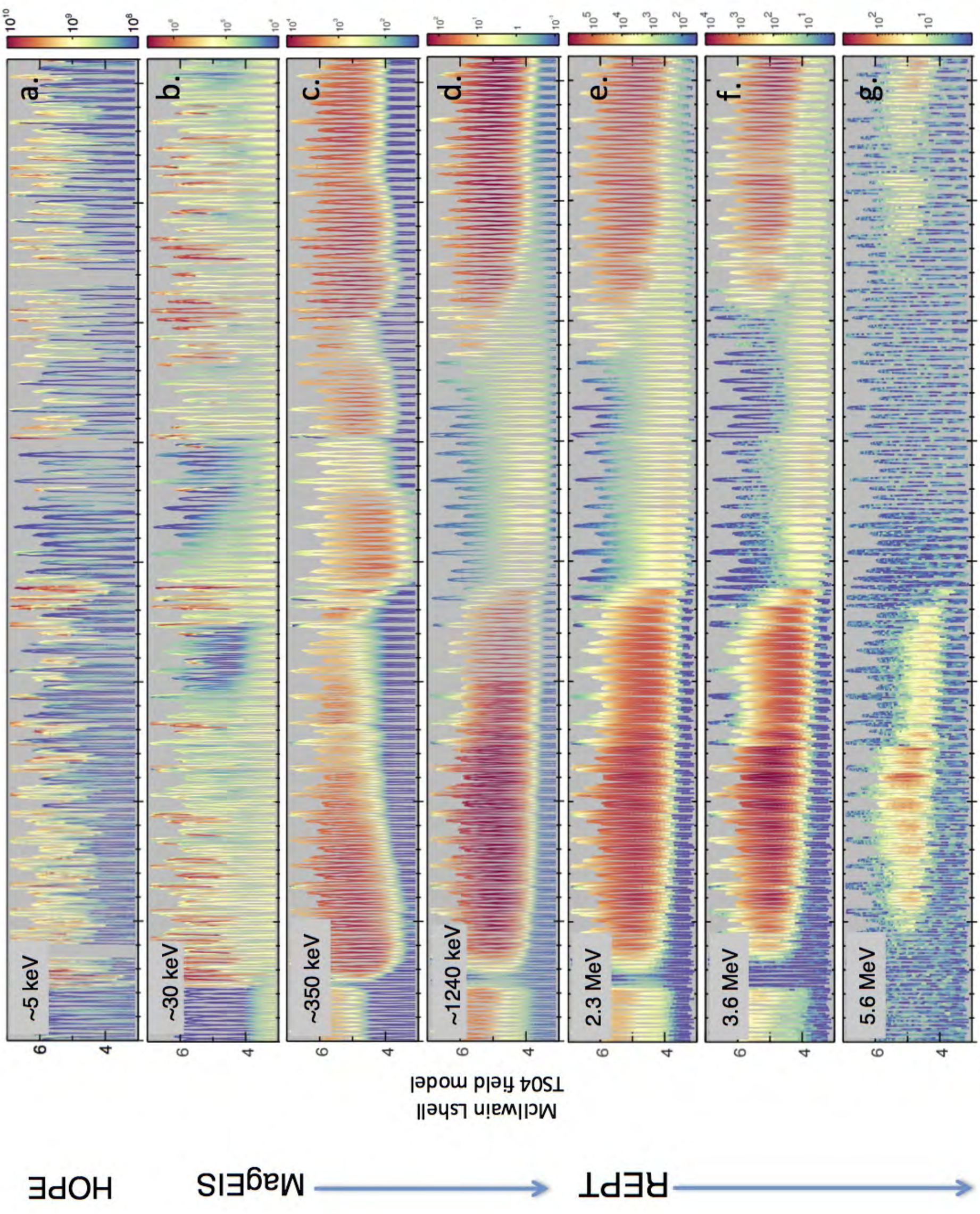
Electron flux (cm² s sr keV)⁻¹
Electron flux (cm² s sr MeV)⁻¹
a.
b.
c.
d.
e.
f.
g.
~5 keV
~30 keV
~350 keV
~1240 keV
2.3 MeV
3.6 MeV
5.6 MeV
L*
McIlwain Lshell
T504 field model
04 Oct 2014
29 Sep 2014
24 Sep 2014
19 Sep 2014
14 Sep 2014
09 Sep 2014
04 Sep 2014
30 Aug 2014
25 Aug 2014
HOPE
MagEIS
REPT

MagEIS-A M75 237 keV

Pitch Angle (degrees)

0.
50.
100.
150.

8000.
6000.
4000.
2000.

cm^{-2} s^{-1} sr^{-1} keV^{-1}

MagEIS-A M75 456 keV

Pitch Angle (degrees)

0.
50.
100.
150.

10^3
10^2
10^1

cm^{-2} s^{-1} sr^{-1} keV^{-1}

REPT-A 2.0 MeV

Pitch Angle (degrees)

0.
50.
100.
150.

10^5
10^4
10^3
10^2

cm^{-2} s^{-1} sr^{-1} MeV^{-1}

19:00
20:00
21:00
22:00
23:00
00:00
2014-09-13
01:00

McIlwain L : TS04 model (R_E)

0.
1.
2.
3.
4.
5.
6.
7.

19:00
20:00
21:00
22:00
23:00
00:00
2014-09-13
01:00

GOES-13 MAGED 30-50 keV

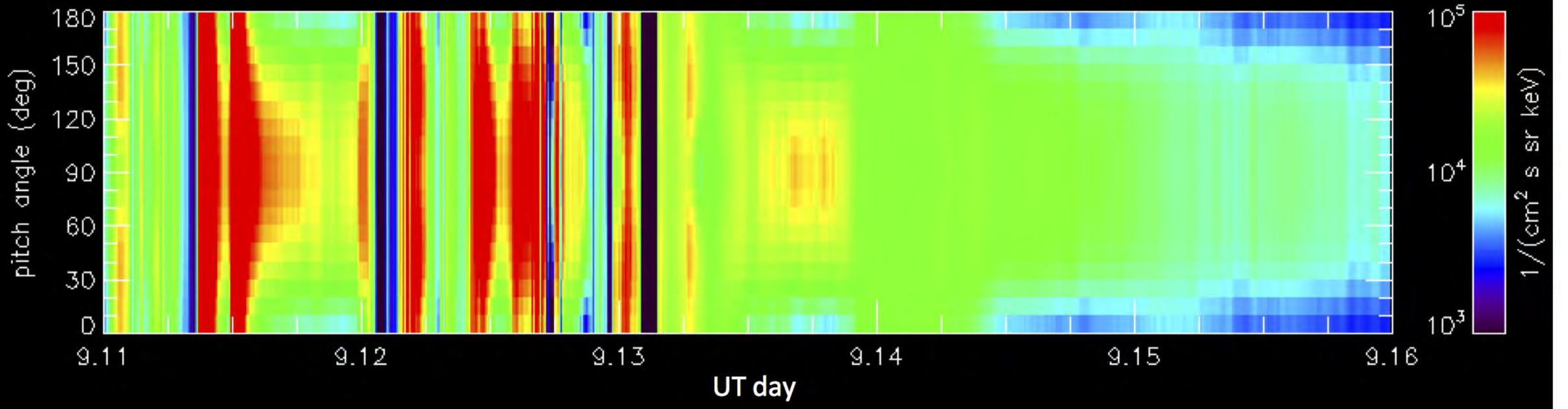

GOES-13 MAGED 50-100 keV

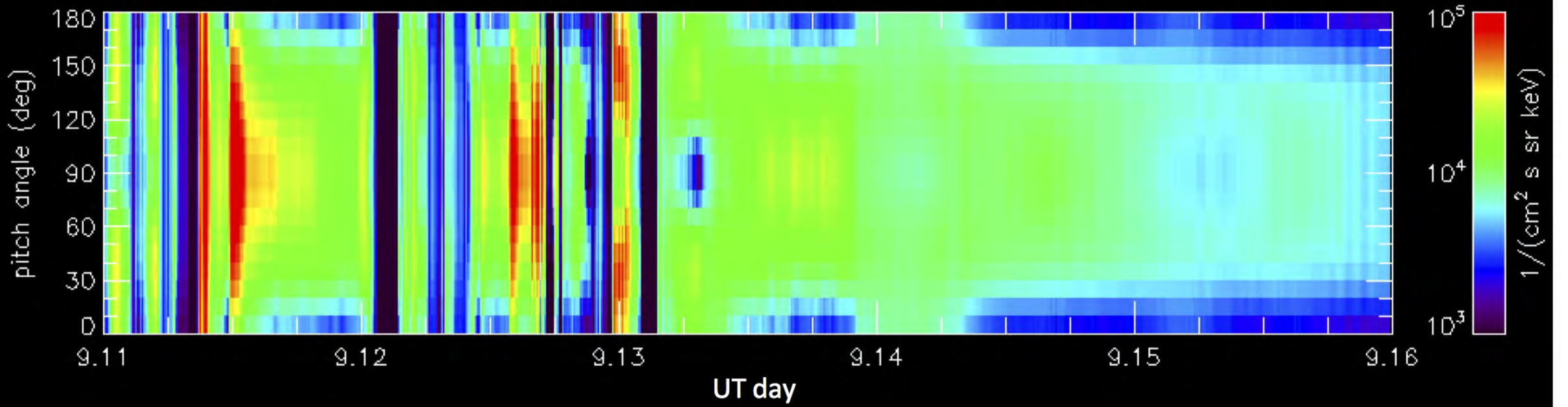

GOES-13 MAGED 100-200 keV

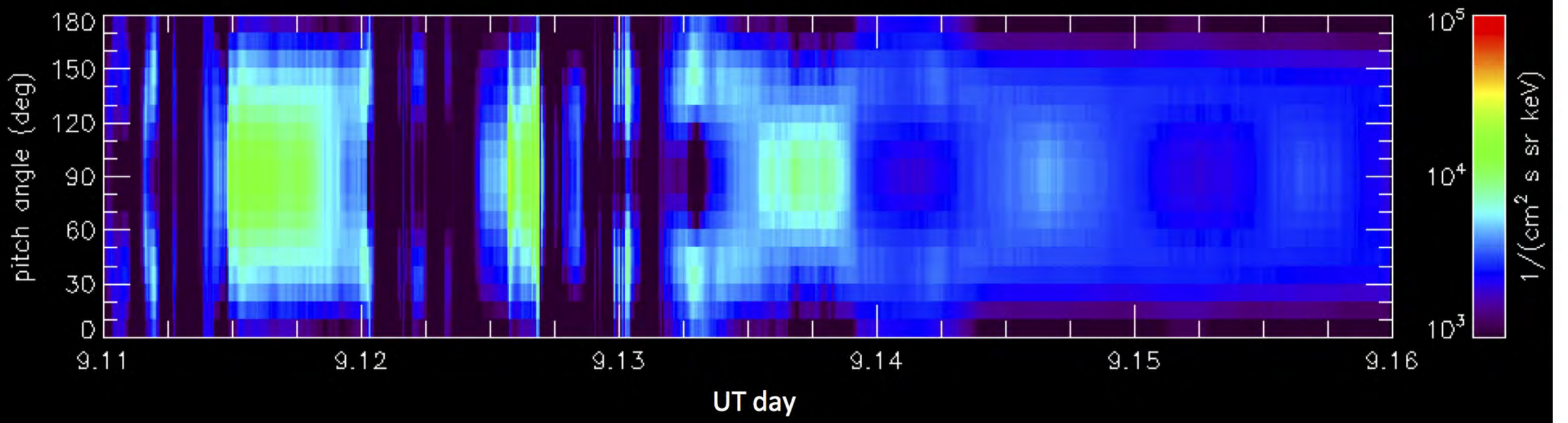

Sep 12-14
MeV loss

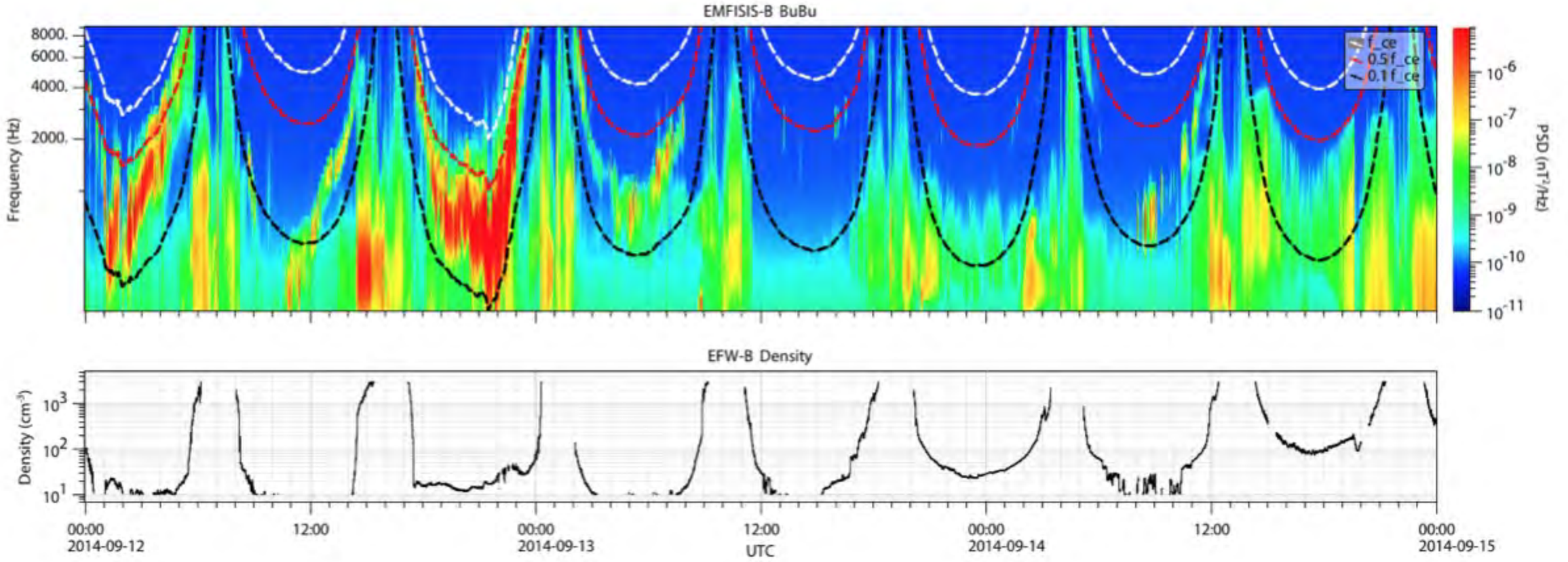

Sep 21-24
MeV reappearance

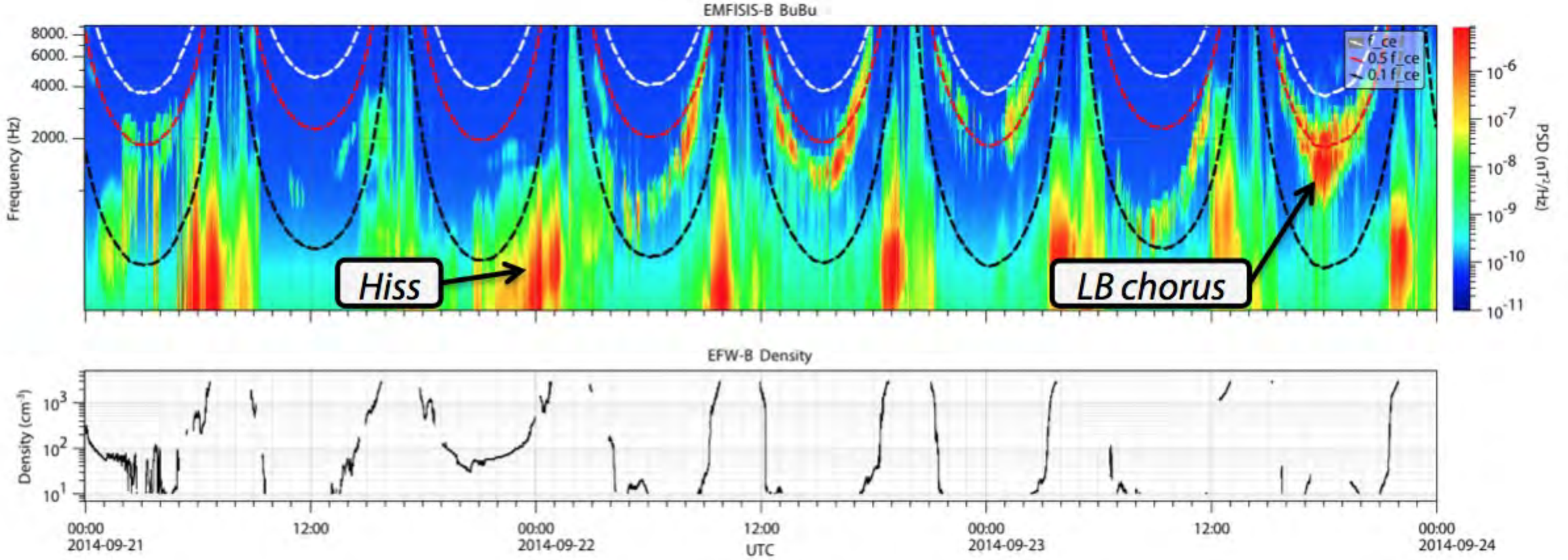

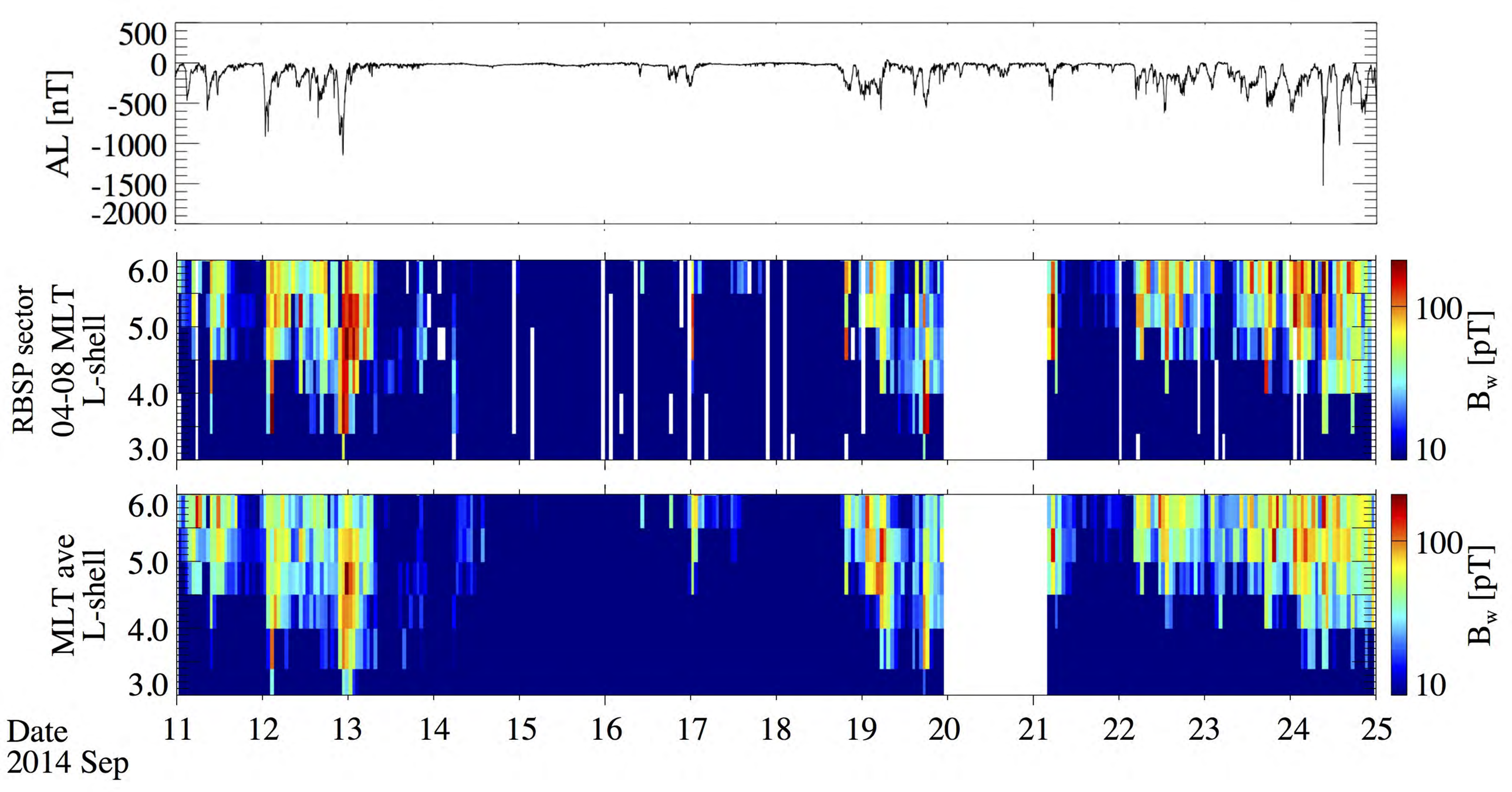
AL [nT]
500
0
-500
-1000
-1500
-2000
RBSP sector
04-08 MLT
L-shell
6.0
5.0
4.0
3.0
100
10
B_w [pT]
MLT ave
L-shell
6.0
5.0
4.0
3.0
100
10
B_w [pT]
Date
2014 Sep
11
12
13
14
15
16
17
18
19
20
21
22
23
24
25

Log of Power Spectral Density - B Compressional - RBSP-A (nT^2/Hz)

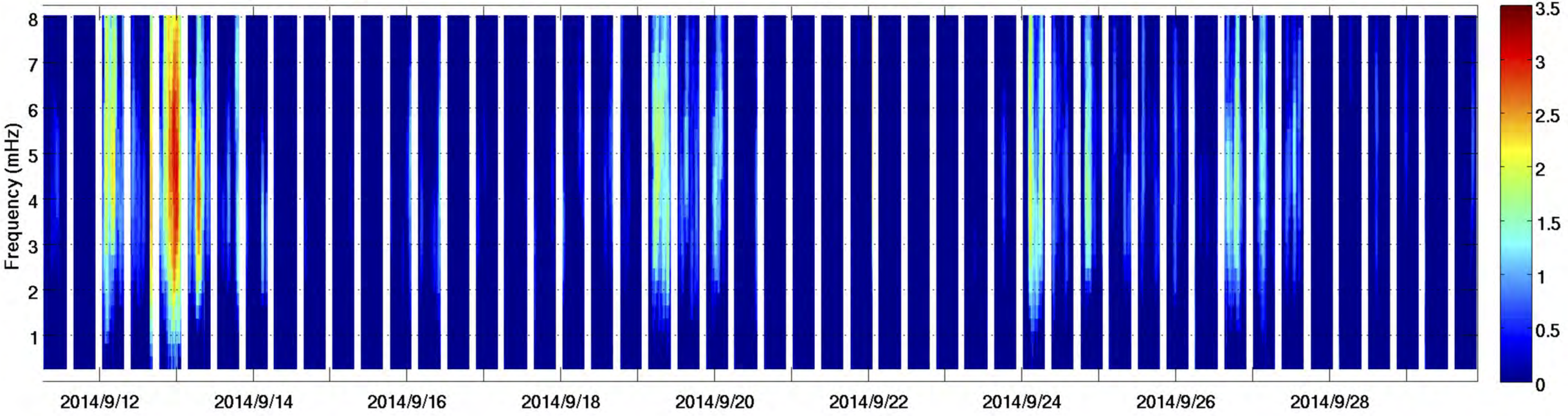

Log of Power Spectral Density - B Compressional - RBSP-B (nT^2/Hz)

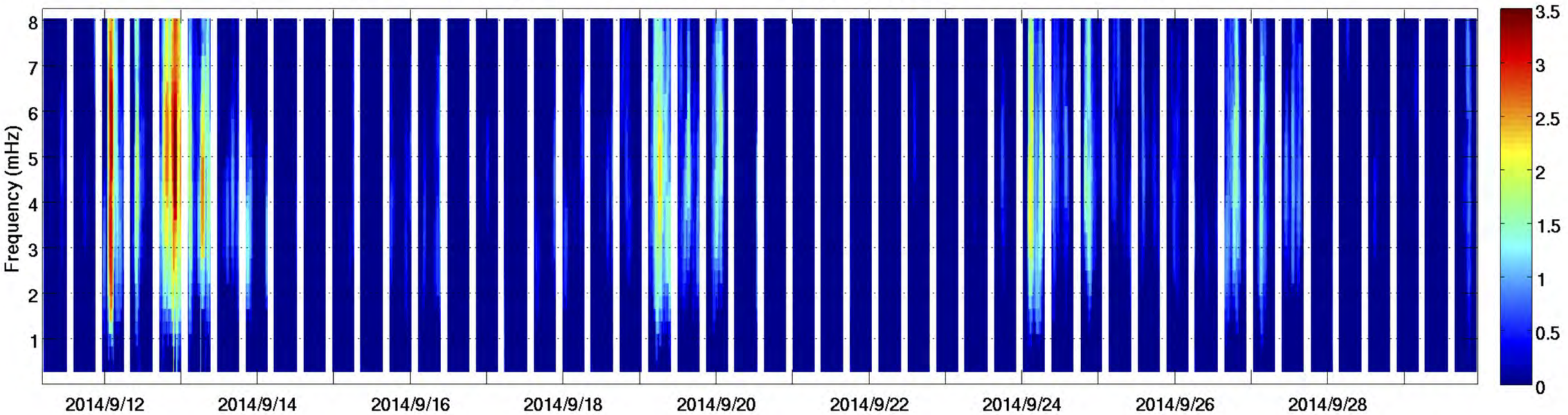

RBSP-A REPT & MagEIS electron spectra : Sept 09-27, 2014 : Outbound pass : Low MLAT

Sept 09 19:34:12-19:43:25 UT
Sept 11 16:26:35-16:35:37 UT
Sept 13 22:16:23-22:25:36 UT
Sept 15 19:12:25-19:21:38 UT
Sept 17 16:04:39-16:13:52 UT
Sept 19 21:55:06-22:04:07 UT
Sept 21 18:50:46-18:59:58 UT
Sept 23 15:42:49-15:52:02 UT
Sept 25 21:33:24-21:42:34 UT
Sept 27 18:28:55-18:38:06 UT

MagEIS
REPT

L=4.5

Flux (cm^{-2} s^{-1} sr^{-1} MeV^{-1})

10^8
10^6
10^4
10^2
1

0.01
0.10
1.00
10.00

Electron Energy (MeV)